Referee (#1)

The authors would like to thank Referee #1 for his/her thoughtful and helpful comments and suggestions. Below are the comments by Referee #1 in blue and our response in black. Any modification made to the text of the manuscript has been highlighted within a green box. The line numbers correspond to the version of the manuscript available for online discussion.

Comment 1

This is basically a theoretical sensitivity study focusing on surface reflectance. Some additional analysis of what to expect in a real retrieval (e.g., Zhou et al., 2010; Lin et al., 2015) and applications (which combine pixels with forward reflecting and pixels with backward reflecting) would be nice. I expect that adding forward and backward scenes together reduce the net effect of surface reflectance on both cloud and NO_2.

Doing a retrieval accounting for the surface BRDF in all the steps is not possible at this stage, as it would require the development of two (cloud and trace gas) retrievals explicitly accounting for surface anisotropy effects, as well as the addition of a model to account for BRDF effects over water. One of the main motivations for our theoretical study was to quantify the effects over land and to confirm that it is strictly necessary to coherently account for surface BRDF both in trace gas and cloud retrievals.

Sections 4.2 and 5.2 describe pseudo-applications, where both forward and backward pixels are considered with the exact same geometry that we encounter in one month of measurements. The spatially averaged result is an increase in the AMF of 6% and 9% over Amazon and France respectively when accounting for surface BRDF effects. As shown by Fig. 11(c, d), averaging over both forward and backward scattering scenes might reduce the net effect for some pixels but not for all of them.

Comment 2

Whether (and how) the effects on Ceff and Mcr act together or compensate each other to affect NO2 AMF is dependent on cloud pressure (CP). In this study, CP is assumed at 850 hPa, which for polluted situations means that most NO2 is below cloud, that Mcd is much smaller than Mcr, and thus that the effects through Ceff and Mcr are complementing each other. A higher CP could lead to Mcd larger than Mcr and thus compensating effects (on NO2 AMF) through Ceff and Mcr. Please comment.

This is a very good point that was not addressed in the manuscript. We have chosen 850 hPa after analysing cloud pressure distributions over Amazonia in March 2008. The distribution for this particular month shows that for low cloud fractions, clouds between 900-800 hPa are more frequent than clouds with pressures between 1000-900 hPa (15% vs. 8%). Over land areas other than Amazonia, this percentage is more similar (22% vs. 19%). A preliminary analysis done with a directional surface LER derived from GOME-2 shows that accounting for surface reflectance anisotropy effects tends to reduce cloud pressures by 40 hPa on average (with differences up to 120 hPa).

We have repeated the analysis in Sect. 5.1 (surface BRDF effects on tropospheric NO_2 air mass factors) using different cloud pressures (from 800 to 978 hPa).

Figure AC1 shows surface BRDF effects on total tropospheric AMF for decreasing cloud pressure, for a cloud fraction of 0.1. For cloud pressures higher than the 850 hPa assumed in the manuscript, the contribution from surface BRDF effects to the change in *M* from the change in cloud fractions becomes smaller. There is a cloud pressure (in Fig. AC1 between 900 and 950 hPa) for which the effects on M_{cr} and on cloud fraction compensate each other. For an even higher cloud pressure (e.g. 978 hPa), M_{cd} is larger than M_{cr} and the sign of the effect changes. In the backward scattering we have lower BRDF AMFs and in the forward scattering higher BRDF AMFs. In the unpolluted situations the differences also become larger for higher cloud pressures.

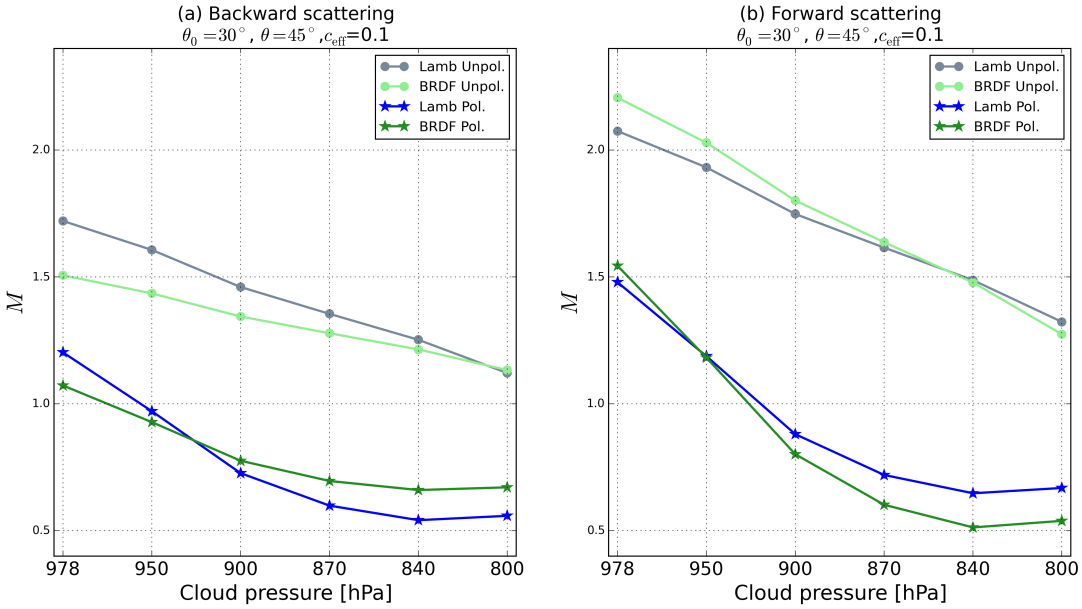

Figure AC1: Total tropospheric NO_2 AMF as a function of cloud pressure in the (a) backward scattering direction and (b) forward scattering direction computed with surface BRDF (green) and a Lambertian surface (blue), for (θ, θ_0) = (45°, 30°), for a moderately polluted (stars) and unpolluted (circles) troposphere. BRDF parameters are (fiso, fvol, fgeo) = (0.04, 0.03, 0.008) and Aws = 0.036 for the Lambertian surface.

We have included Fig. AC1 in the supplementary material, and we have added a paragraph based on the discussion above (P20, L6):

The differences between BRDF and Lambertian AMF for different cloud pressures are shown in Fig. S6 in the supplementary material. A preliminary analysis done with a directional surface LER derived from GOME-2 shows that accounting for surface reflectance anisotropy effects reduces the cloud pressure by 40 hPa on average (with differences up to 120 hPa). This means that high cloud fractions will occur less often

and therefore the results shown for 850 hPa are representative of the surface BRDF effects on AMFs.

Comment 3

Sects. 4 and 5 – Do you assume Henyey-Greenstein clouds in the forward model (Eq. 8) and then assume Lambertian clouds in the reverse model (i.e., in the cloud and NO2 retrievals)? What else are different between the forward and reverse models?

The assumption of the Henyey-Greenstein (HG) cloud is used to simulate top-of-atmosphere radiances with DAK that resemble as much as possible what the satellite would measure (R_{meas}) in a realistic cloudy scene. We then indeed assume Lambertian clouds in the reverse model. In other words, the forward model to simulate TOA radiances assumes surface reflectance to be anisotropic, and includes a HG cloud, and the reverse model assumes the cloud reflection to be Lambertian. The assumption of a Lambertian cloud is what is currently done in the operational cloud retrievals at KNMI (O2-O2, FRESCO+).

We have modified the sentence that refers to this in the manuscript (P15, L6):

"…we use the forward model DAK to approximate R_{meas} simulating the TOA reflectance for a scene with a Henyey-Greenstein cloud and surface reflectance anisotropy."

Is cloud pressure the same between forward and reverse models?

In our case, the Lambertian cloud is located at the same pressure level as the Henyey-Greenstein cloud (1-2 km). By setting the clouds at the same altitude, we isolated the surface BRDF effects on cloud fraction only, as we do not consider potential effects on cloud pressure.

We have modified Table 1 to include this information and clarify the settings of the forward model and inverse simulations.

Table 1. Settings for Lambertian and BRDF c_{eff} simulations in Sect. 4.1. Inverse model for Lambertian c_{eff} reproduces current O_2-O_2 and FRESCO+ retrievals, with Lambertian surface and Lambertian cloud. Inverse model for BRDF c_{eff} reproduces the retrieval accounting for surface BRDF effects.

Forward model, R_{meas}		**Inverse model, c_{eff}**	
Henyey-Greenstein scattering cloud		**Lambertian cloud (R_{cd})**	
Asymmetry parameter, g	0.85	Cloud albedo, A_{cd}	0.8
Cloud optical thickness, τ_c	30	Cloud altitude	1-2 km
Cloud altitude	1-2 km	**Lambertian c_{eff}: surface albedo (A_{ws}) for R_{cr}**	
Geometric cloud fraction, c_{geo}	0, 0.05, 0.2, 0.5	λ = 477 nm	0.0217
Surface reflectance: BRDF parameters (f_{iso}, f_{vol}, f_{geo}) for R_{cr}		λ = 758 nm	0.337
λ = 477 nm	0.03, 0.02, 0.01	**BRDF c_{eff}: surface parameters (f_{iso}, f_{vol}, f_{geo}) for R_{cr}**	
λ = 758 nm	0.4, 0.25, 0.08	λ = 477 nm	0.03, 0.02, 0.01
		λ = 758 nm	0.4, 0.25, 0.08

We have added a sentence in the text (P15, L18):

The Lambertian cloud is located at the same pressure level as the Henyey-Greenstein cloud so we can isolate surface BRDF effects on cloud fraction only (see settings in Table 1).

It is not clear how the difference between Ceff and Cgeo is derived. Also, where is the Cgeo from (e.g., in Fig. 8)?

In cloud retrievals, the difference between geometric and effective cloud fraction, as explained in Stammes et al. (2008):
"The effective cloud fraction is the amount of Lambertian cloud with albedo Ac that one has to add to the clear pixel to explain the observed reflectance. The geometric cloud fraction is the part of the pixel that is covered by the "true" cloud. The effective cloud fraction is the radiometrically equivalent cloud fraction, which in combination with the assumed cloud albedo yields a TOA reflectance that agrees with the observed reflectance."

In Sect. 4.2 (Fig. 8), in order to apply Eq. 8, we used a C_{geo} distribution with an area-wide average of 0.33 distributed randomly for East and West measurements (Fig. 8a, d). Together with the Henyey-Greenstein cloud simulation, we applied Eq. 8 to obtain R_{meas} using those C_{geo} values. Finally, we apply Eq. 9 to obtain the effective cloud fraction (C_{eff}) (with Lambertian and BRDF assumptions, Fig. 8 b,e,c,f).

We have slightly modified the text that explains this (P17, L5):

To simulate measured reflectance, we assume a geometric cloud fraction distribution with an area-wide average of C_{geo} = 0.33. Figure 8a,d show the C_{geo} distribution for East and West measurements respectively.

Comment 4

P3, L20 – clarify "clear-sky"

Clear-sky means that they only selected scenes where cloud fraction was very low or strictly zero (Noguchi et al., 2014). We modify the sentence:

"They analyzed clear-sky scenes (i.e. no clouds present) or scenes with very low cloud fractions (i.e. lower than 0.2), ..."

Comment 5

P12, L7 – could you comment on the large difference near the hot-spot region between LIDORT and DAK/SCIATRAN?

We did not address this issue in the manuscript as the only purpose of the comparison with LIDORT and SCIATRAN was to validate our surface BRDF implementation in DAK. The reason for the difference between LIDORT and DAK, SCIATRAN is that there is no hot-spot correction in the simulations by LIDORT (H. Yu, personal communication).

Comment 6

Sect. 5.1 – why not use the retrieved Ceff_BRDF, rather than assuming Ceff_BRDF = 0.1 ± 0.05?

In Sect. 5.1 we use a fixed change in the cloud fraction to understand how the change in cloud fraction due to surface BRDF affects forward and backscatter measurements separately. The choice of 0.1 ± 0.05 is our best approximation of what would happen if we develop a completely new revised cloud algorithm based our analysis in Sect. 4. In Sect. 5.2, we use the calculated Ceff_BRDF from section 4.2 (shown in Fig. 8) and not the fixed change of ± 0.05.

We modify the text to make it clear (P20, L12):

We apply Lambertian and BRDF C_{eff} distributions from Sect. 4.2 (as in Fig. 8). This way we account for the calculated surface BRDF effects in cloud fraction instead of the average change of 0.05 assumed in the sensitivity analysis in Sect. 5.1.

Comment 7

Table 2 –please provide a complete set of ancillary parameters such Ps, T profile, etc.

Atmospheric profile corresponds to the mid latitude standard atmosphere (Anderson et al., 1986). We extend Table 2 with this information. Fig. AC2 shows the NO_2 profiles that were used for the moderated polluted and unpolluted simulations in Sect. 4. These profiles correspond to $N_{v,trop} = 4 \cdot 10^{15}$ molec/cm^2 and $N_{v,trop} = 0.2 \cdot 10^{15}$molec/cm^2.

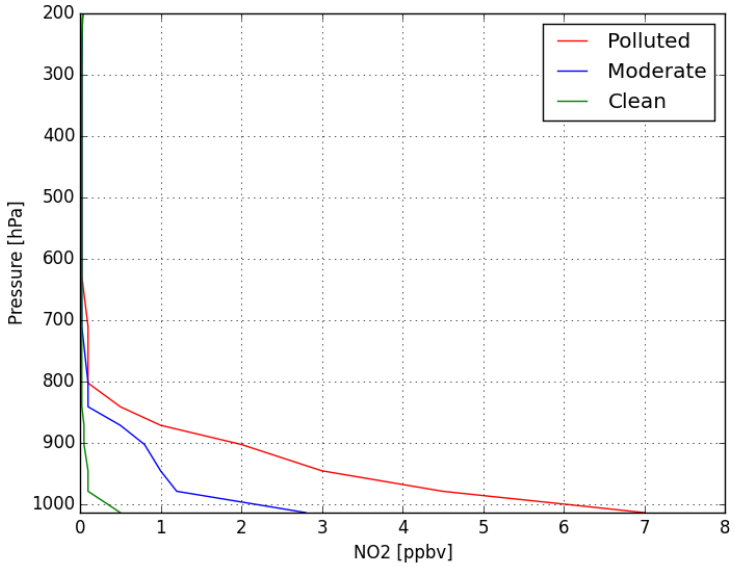

Figure AC2: Clean, moderate and polluted profiles used in the study.

References

Anderson, G. P., Clough, S. A., Kneizys, F. X., Chetwynd, J. H., and Shettle, E. P.: AFGL Atmospheric Constituent Profiles (0– 120 km), Environ. Res. Papers, Optical Physics Division, Air Force Geophysics Laboratory Hanscom AFB, MA, 43 pp., http://nla.gov.au/nla.cat-vn4005592, 1986.

Noguchi, K., Richter, A., Rozanov, V., Rozanov, A., Burrows, J. P., Irie, H., and Kita, K.: Effect of surface BRDF of various land cover types on geostationary observations of tropospheric NO2, Atmos. Meas. Tech., 7, 3497–3508, https://doi.org/10.5194/amt-7-3497-2014, 2014.

Referee (#2)

The authors would like to thank Referee #2 for his/her thoughtful and helpful comments and suggestions. Below are the comments by Referee #2 in blue and answers in black. Any modification made to the text has been highlighted within a green box. The line numbers correspond to the version of the manuscript available for online discussion.

Comment 1

Almost all analyses are made for a domain over the Amazon forest. This choice is never motivated. In terms of NO_2, this is not the most relevant region I can think of.

The motivation to show the analysis over the Amazon forest was that the surface LER across track dependency is very strong over that region, and there are occasionally elevated amounts of NO_2 associated with biomass burning. Figure AC1 shows that surface LER directionality is also very strong over similar regions like Equatorial Africa, and it is also relevant over Asia.

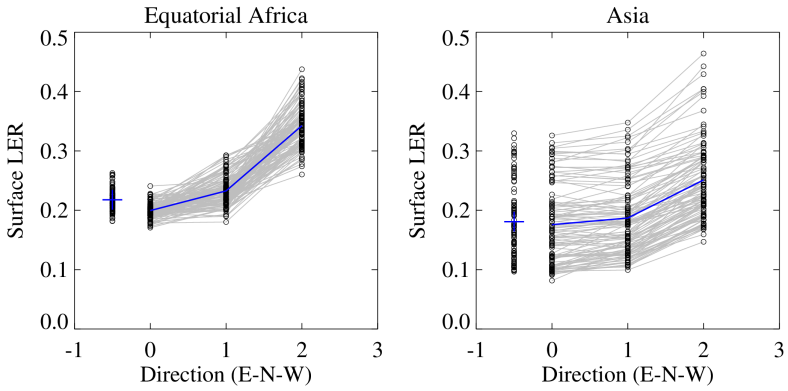

Figure AC1: Directional dependence of surface LER climatology (2007-2013) derived from individual measurements along the swath: East (E) for the 8 easternmost pixels, Nadir (N) for the 8 center pixels and West (W) for the 8 westernmost pixels. (Same as Fig. 1d in the manuscript).

When we analysed the retrieved cloud fractions over the Amazon, we found a strong East-West across track bias, so we decided to focus on that region. We also found important biases in other regions like France (Fig. AC2), which we also investigated in detail.

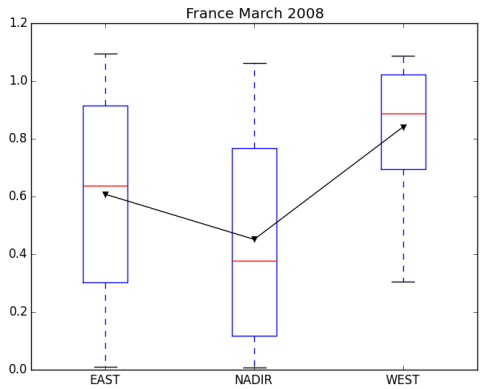

Figure AC2: Box-plot of cloud fractions retrieved with FRESCO cloud retrieval for GOME-2A for March 2008 over France (Lat:44-49N, Lon:0-6W).

Comment 2

Because of the focus on this forested region, the analyzed BRDF effects may be larger than over other regions of the globe with less dense and tall vegetation. This should be better emphasized in the paper (e.g. in the abstract). In the discussions and conclusions section on page 23, line 3, for example, it is mentioned that surface albedo is underestimated by as much as a factor 2 over "vegetated" scenes, but "vegetated" in this case actually means forested. Results would likely be quite different over other vegetated surfaces like grass- or croplands.

We agree, so have changed the term vegetated in Sect. 6. and in other relevant sentences and we have included the term “forest” in the abstract to emphasize that the larger cloud fraction bias found in the analysis is over Amazonia.

We agree that the results might be different over other vegetated regions, but in order to make concluding statements about the effects over different land cover types, a global analysis would be needed. That we also find cloud fraction bias over France, and that the differences in NO2 AMFs are also substantial there, suggests that the effects are relevant also over non-forested surfaces. The study by Noguchi et al. (2014), addressing different land cover types, showed that all land types show a similar behaviour on the surface BRDF (Fig. 7 from Noguchi et al. (2014)).

Comment 3

GOME-2 and OMI have different equator crossing times (GOME-2 has a morning, OMI and after-noon orbit), an information that seems missing in the manuscript but is relevant for the interpretation of the results. Because GOME-2 is further away from noon, I would expect BRDF effects to be larger for GOME-2 than for OMI.

This is a very good point. However, we think that from our study the conclusion that BRDF effects are larger for GOME-2 than for OMI due to the different equator crossing time cannot be made. The fact that cloud fraction across-track dependency is stronger for GOME-2 than for OMI is more likely to be related to the spectral region used for

the cloud retrievals. The major difference between cloud fractions from OMI and GOME-2 is the spectral window from which they are retrieved. That GOME-2 retrieves clouds in the NIR, where the atmosphere is more transparent than in the VIS and surface BRDF effects are stronger, makes FRESCO more sensitive to surface BRDF. Furthermore, OMI pixels are smaller, so it is less likely that BRDF effects are smeared out as in the larger GOME-2 pixels. The study by Noguchi et al. (2014) suggested that, for a geostationary sensor, BRDF effects are not weaker in the morning when the RAA is low compared to the afternoon when RAA is high. We conclude that the strength of the BRDF-effect depends mostly on the specific relative position of the sun and the satellite, and on the spectral range where the retrievals are done.

Comment 4

The study emphasizes the importance of satellite missions that can provide surface BRDFs like MODIS. Since the MODIS missions have surpassed their designed lifetime already by far, the community should think about alternatives for the post-MODIS period. Can the Sentinels fill this gap? Maybe this would be worth a sentence in the discussions section.

This is a good point that we should keep in mind. Below we provide a short summary of current and future Land Earth Observation capabilities, and we added few sentences in the last paragraph of the discussion (Sect. 6).

MODIS-Terra is expected to last until 2022 and has sufficient fuel to last until 2030. MODIS-Aqua can stay in the same orbit until 2025 and may have enough fuel possibly until 2035. Suomi NPP-VIIRS (Visible Infrared Imaging Radiometer Suite, and JPSS-VIIRS) now produce a MODIS-like BRDF (a fixed 16-day window updated daily). This constellation assures continuity of land data until 2038.

From the Copernicus Sentinels, Sentinel-3 could be employed to generate a BRDF similar to the one from the ESA GlobAlbedo broadband and the QA4ECV spectral albedo product after some years of measurements.

Modification to last paragraph in Sect. 6:

A viable alternative to the current LER climatologies is provided by the MODIS-derived BRDF-parameters at a spatial resolution better than the GOME-2, OMI, and TROPOMI pixel sizes. MODIS Terra and Aqua are expected to last until 2025 and afterwards the Joint Polar Satellite System (JPSS) satellite constellation assures continuity of land observations needed to produce surface BRDF data. Sentinel-3 could be employed to generate a BRDF similar to the one from the ESA GlobAlbedo broadband and the QA4ECV spectral albedo after some years of measurements. Another alternative is to make a directionally dependent LER database from TROPOMI once there is enough surface reflectance data acquired by the satellite itself.

Short comments by W. Qin

We thank W. Qin for the comments on our manuscript. Below are the comments in blue and our response in black. Any modification made to the text of the manuscript has been highlighted within a green box. The line numbers correspond to the version of the manuscript available for online discussion.

Comment 1

The paper misrepresents the GLER product (Vasilkov et al., 2017) as GLER climatology (line 15, page 3). GLER is not a climatology, but a bidirectional (sun-view geometry dependent) LER product at a scale of satellite pixel (OMI is used as an example). GLER is derived using real OMI pixel geometry and MODIS high-resolution BRDF product over land averaged over an OMI field of view (FOV) and the Cox-Munk slope distribution over ocean with a contribution of water-leaving radiance. This is the kind of product the authors recommended for TROPOMI in the conclusion section.

We apologize for the misrepresentation by the use of the term climatology. We have modified that.

"Vasilkov et al. (2017) created a geometry dependent surface LER (GLER) product"

Comment 2

The authors implemented MODIS BRDF model into the RT DAK and use it for UV/Vis wavelengths of OMI and GOME-2 (section 3.2, see line 30, page 11). It is not clear if DAK is a scalar or vector RT model in terms of atmospheric RT simulation. But the models that DAK is compared to for evaluation include a scalar model (LIDORT) and a model (SCIATRAN) that has both modes (scalar or vector), and which mode is used is not clear either. However, as indicated in Vasilkov et al, 2017, our experience with VLIDORT has shown that ignoring polarization for UV wavelengths would result up to 10% error in TOA radiance simulations.

DAK is capable of simulating radiative transfer in the atmosphere with and without accounting for polarization. The simulations shown in the comparison do not account for polarization. The only purpose of the comparison with LIDORT and SCIATRAN was to assure that surface BRDF was correctly implemented into DAK. Therefore we did not give many details on the settings of the radiative transfer simulations. We have now added a sentence that gives some information on the main settings (P11, L32):

These settings include no polarization, a plane parallel standard mid-latitude atmosphere and absorption by O3, O2-O2.

Comment 3

The operational MODIS product (MCD43A1) is used in this paper for surface BRDF characterization (line 15, page 11). However, as we know, operational MODIS BRDF product usually has up to 20% gaps globally due to cloudiness. That's why we use gap-filled MODIS product (MCD43GF) in our GLER product.

The surface BRDF parameters used in the simulations in Sect. 3 (Figs. 4, 5 and 6) from MCD43A1 MODIS product are the spatial average over Amazonia. We used it as an example of combination of f_{iso}, f_{vol} and f_{geo} for surface and TOA reflectance simulations in Sect. 3. Because it was spatially averaged we did not worry about the gaps that the product might have. In the following sections, we used a climatology created by the QA4ECV Land group (page 15, line 10). This climatology is a daily climatology based on 16 years of measurements (2000-2016).

Comment 4

This paper only covers BRDF effects on NO_2 and cloud products (FRESCO and OMCLDO2) over land, and ocean is not mentioned at all. But ocean reflection is nonLambertian either. A good example is the sunglint effect caused by Fresnel reflection, which creates strong forward reflection as significant as the so-called hot-spot effect in the backward scattering direction over land as discussed in this paper. To characterize the surface BRDF effect globally, one has to consider both land and ocean.

We fully agree with the importance of the ocean and the necessity of accounting for ocean reflection in a global retrieval that fully accounts for surface BRDF effects. However, for our study the main focus was over land, so we did not take ocean into account. Regarding the radiative transfer model DAK, the next step to take is to implement the Cox-Munk model for sea surface reflectance.

Comment 5

It is mentioned in couple of places (line 5, page 1; line 11, page 21) that rugged terrain causes strong backscattering reflection. However, not only rugged terrain, any rough surfaces like vegetation and soils produce strong backscattering, even the terrain is flat.

We have modified the term rugged terrain from the abstract (P1, L5). In this case we were referring to forested area (Amazon) where we found the highest cloud fraction bias. In page 21, line 11 we also meant forested terrain, so we have also changed the term “rough terrain”.

Comment 6

The discontinuity of the green curve at nadir in Fig.9b indicates something is not correct in the simulations, which needs more explanation.

The discontinuity in Fig. 9b is because in the forward scattering regime (positive ϑ) we assume an increase in the cloud fraction and in the backward scattering regime (negative ϑ) we assume a decrease. This means that cloud fractions in Eq. 12 are different for each scattering regime, causing the “discontinuity” in the cloud radiance fraction (Fig. 9b) and in the total AMF (Fig. 9c) when $\vartheta = 0°$.

The importance of surface reflectance anisotropy for cloud and NO_2 retrievals from GOME-2 and OMI

Alba Lorente[1], K. Folkert Boersma[1,2], Piet Stammes[2], L. Gijsbert Tilstra[2], Andreas Richter[3], Huan Yu[4], Said Kharbouche[5], and Jan-Peter Muller[5]

[1]Wageningen University, Meteorology and Air Quality Group, Wageningen, the Netherlands.
[2]Royal Netherlands Meteorological Institute (KNMI), De Bilt, the Netherlands.
[3]Institute of Environmental Physics (IUP-UB), University of Bremen, Bremen, Germany.
[4]Belgian Institute for Space Aeronomy (BIRA-IASB), Brussels, Belgium.
[5]Imaging Group, Mullard Space Science Laboratory, Department of Space and Climate Physics, University College London, Holmbury St Mary, UK.

Correspondence: A. Lorente (alba.lorentedelgado@wur.nl)

Abstract. The angular distribution of the light reflected by the Earth's surface influences top-of-atmosphere (TOA) reflectance values. This surface reflectance anisotropy has implications for UV/Vis satellite retrievals of albedo, clouds, and trace gases such as nitrogen dioxide (NO_2). These retrievals routinely assume the surface to reflect light isotropically. Here we show that cloud fractions retrieved from GOME-2A and OMI with the FRESCO and OMCLDO2 algorithms have an East-West bias of 10% to 50%~~over rugged terrain~~, highest over vegetation and forested areas, and that this bias originates from the assumption of isotropic surface reflection. To interpret the across-track bias with the DAK radiative transfer model, we implement the Bidirectional Reflectance Distribution Function (BRDF) from the Ross-Li semi-empirical model. Testing our implementation against state-of-art RTMs LIDORT and SCIATRAN, we find that simulated TOA reflectance generally agrees to within 1%. By replacing the assumption of isotropic surface reflection in the cloud retrievals over ~~vegetated~~ forested scenes with scattering kernels and corresponding BRDF parameters from a daily, high-resolution database derived from 16 years' worth of MODIS measurements, the East-West bias in the retrieved cloud fractions largely vanishes. We conclude that across-track biases in cloud fractions can be explained by cloud algorithms not adequately accounting for the effects of surface reflectance anisotropy. The implications for NO_2 air mass factor (AMF) calculations are substantial. Under moderately polluted NO_2 and backscatter conditions, clear-sky AMFs are up to 20% higher and cloud radiance fractions up to 40% lower if surface anisotropic reflection is accounted for. The combined effect of these changes is that NO_2 total AMFs increase by up to 30% for backscatter geometries (and decrease by up to 35% for forward scattering geometries), stronger than the effect of either contribution alone. In an unpolluted troposphere, surface BRDF effects on cloud fraction counteract (and largely cancel) the effect on the clear-sky AMF. Our results emphasize that surface reflectance anisotropy needs to be taken into account in a coherent manner for more realistic and accurate retrievals of clouds and NO_2 from UV/Vis satellite sensors. These improvements will be beneficial for current sensors, in particular for the recently launched TROPOMI instrument with a high spatial resolution.

1 Introduction

Nitrogen dioxide (NO_2) in the lower troposphere is an important constituent of air pollution. In Europe, the annual mean NO_2 concentration limit value (40 $\mu g/m^3$) is still widely exceeded, exposing 30 million people to poor air quality with known harmful health effects (EEA, 2016). In combination with other pollutants and sunlight, chemical and physical transformations of nitrogen oxides ($NO+NO_2=NO_x$) lead to the formation of particulate matter and ozone smog, further impacting public health, ecosystems, and climate. Satellite measurements of tropospheric NO_2 column densities provide much better spatial coverage than ground-based sensors, and they have been used to monitor trends, and to estimate NOx emissions and NO_2 surface concentrations (e.g. Richter et al. (2005), Martin et al. (2003), Lamsal et al. (2008)). The spatial resolution of the satellite instruments and their retrievals is improving such that the observed NO_2 pollution can now be traced back to emissions from individual cities, power plants, and transportation sectors. The uncertainty of satellite NO_2 retrievals is considerable, and mainly related to the adequacy of the assumptions made on the state of the atmosphere. We recently estimated the structural uncertainty from an ensemble of NO_2 retrievals to be on the order of 30-40% (Lorente et al., 2017). An important component of this uncertainty is how surface properties (usually from an external database) are taken into account, and how errors in the external database propagate in the air mass factor (AMF) calculations. This is not straightforward, because the AMF calculation directly depends on surface properties under clear-sky circumstances, and indirectly via cloud parameters retrieved for the same scene by the cloud algorithm.

Surfaces reflect light differently in each direction, and the angular distribution of the reflected light influences top-of-atmosphere (TOA) reflectance levels measured by satellite instruments that monitor atmospheric composition. Therefore, surface reflectance anisotropy influences retrievals of surface albedo, trace gases, aerosols and clouds from satellite instruments like the Global Ozone Monitoring Experiment 2 (GOME-2) and the Ozone Monitoring Instrument (OMI). In surface albedo, cloud, aerosols and trace gas retrievals, the surface is often assumed to be Lambertian: an idealized surface that reflects light isotropically (e.g. Kleipool et al. (2008), Veefkind et al. (2016), Torres et al. (2007), Boersma et al. (2011)). This assumption implies that the geometry dependent scattering properties of the reflecting surface are ignored.

The so-called Lambertian-equivalent-reflectivity (LER) climatologies represent the albedo of the Lambertian surface in the radiative transfer simulations for cloud retrievals and trace gas retrievals. In constructing such climatologies (e.g. monthly climatologies), a large ensemble of measurements taken over a scene over multiple years is analyzed statistically, and based on the lower 1% percentile reflectance, an inversion is done to retrieve the surface reflectance (e.g. Koelemeijer et al. (2003), Kleipool et al. (2008), Tilstra et al. (2017)). Depending on the exact viewing and illumination geometry however, the surface may appear darker or brighter. Taking the lower 1% percentile reflectances therefore skews the distribution of retrieved albedo values to those scenes that appear darker from space. Using these climatologies therefore fails to represent any surface reflectance anisotropic effects on TOA reflectance simulations for the widely varying subset of viewing geometries encountered along a satellite orbit. We may expect cloud retrievals to be directly affected by the assumption of a Lambertian surface in the radiative transfer: if a scene is brighter than predicted by the biased climatology, cloud fractions will be overestimated. Trace gas retrievals are affected by the Lambertian assumption in the calculation of the AMF: directly via the clear-sky AMF and

also indirectly because the retrieved cloud parameters are used to correct for the possible presence of residual clouds via the independent pixel approximation (IPA) method. In the IPA, the cloud radiance fraction weighs the clear-sky and cloudy parts of the scene for the calculation of the overall AMF and vertical column density (VCD) (e.g. Martin et al. (2002)).

The angular distribution of the reflected light by a surface is represented mathematically by the Bidirectional Reflectance Distribution Function (BRDF) (Nicodemus et al., 1992). Anisotropy is a fundamental physical property of surface reflectance, so in order to fully represent the geometry dependent surface scattering properties in cloud and trace gas retrievals, surface BRDF has to replace the isotropic Lambertian albedo. Some studies have already shown that surface BRDF effects are important for NO_2 and cloud retrievals. Zhou et al. (2010) found that after including surface BRDF over Europe, differences in NO_2 columns were higher in November (20%) compared to July (3%), when the solar zenith angle is small. Noguchi et al. (2014) studied surface BRDF effects on the diurnal cycle of clear-sky geostationary measurements over Japan, and found that whether NO_2 columns are under (-15%) or overestimated (+9%) depends on the specific geometry of the measurement. To also address the need of including surface BRDF effects on cloud algorithms, Lin et al. (2014, 2015) updated the POMINO retrieval over China. Changes in surface reflectance led to changes of opposite sign in cloud fraction (±0.05) and more complex effects on cloud pressure, with an overall change of 10% in NO_2 columns that were regionally and seasonally dependent. Vasilkov et al. (2017) ~~calculated~~ created a geometry dependent surface LER (GLER) ~~climatology~~ product and applied it to OMI NO_2 and cloud retrievals. They found relatively small effects on retrieved cloud parameters and relatively high differences in retrieved NO_2 columns (up to 50%) driven by GLER values being on average smaller than the original LER.

These studies show that surface BRDF effects depend on the specific geometry (hence local time and season) and surface characteristics of the individual measurements, and that averaging over many pixels results in smaller differences. They analyzed mostly clear-sky ~~situations~~scenes (i.e. no clouds present) or scenes with very low cloud fractions (i.e. lower than 0.2), and they did not consider how surface reflectance anisotropy affects the radiative transfer in the atmosphere and TOA reflectances. The indirect effect of biased cloud parameters on NO_2 retrievals combined with effects on clear-sky AMFs received less attention. Vasilkov et al. (2017) and Lin et al. (2015) addressed the indirect effects and showed that the effects on cloud parameters could enhance or compensate the direct effect on clear-sky AMFs.

Here we study the effect of surface reflectance anisotropy on surface LER climatologies, on cloud fraction retrievals and on NO_2 tropospheric AMFs, covering the essential steps from the TOA reflectance to retrieve the final NO_2 tropospheric column in a partly cloud covered pixel. We present observational evidence that surface reflectance anisotropy skews LER climatologies to the darkest scenes corresponding with forward scattering geometries (Sect. 2). We demonstrate that using these LER climatologies in cloud retrieval algorithms leads to considerable across-track biases in cloud fractions, especially for the ~~O2-A~~ O_2-A band (GOME-2), but also for the 477 nm ~~O2-O2~~ O_2-O_2 band (OMI). In Section 3 we describe our extension of the DAK radiative transfer model (RTM) to include surface reflectance anisotropy with the Ross-Li BRDF semi-empirical model. We validate DAK with state-of-the-art radiative transfer models and evaluate TOA reflectance simulations including surface BRDF at the relevant wavelengths for cloud and NO_2 retrievals. In Sect. 4 we study the consequences of including surface BRDF in the calculation of effective cloud fractions. In Sect. 5 we study the surface BRDF effects on NO_2 AMFs, and

how these, in combination with the effects on cloud fractions, affect tropospheric NO_2 retrievals in cloudy scenes. We end with conclusions and outlook.

2 Evidence of the influence of surface reflectance anisotropy on LER climatologies and cloud retrievals

Surface LER climatologies are commonly used as boundary conditions for cloud and trace gas retrievals (e.g. De Smedt et al. (2017), Bucsela et al. (2013)). Earlier instruments like GOME and SCIAMACHY have very coarse pixels (40 x 320 km^2 and 60 x 30 km^2, respectively) and a narrow swath (960 km). For retrievals from these instruments, the Lambertian assumption can be justified as surface BRDF effects are likely to smooth out over the large and heterogeneous pixels. Newer instruments like OMI, and especially TROPOMI, have a higher spatial resolution (13 x 24 km^2 and 3.5 x 7 km^2, respectively) and a wider swath (up to 2600 km), i.e. a wider range of viewing directions, and therefore the surface BRDF effects become more relevant. One of the advantages of using LER climatologies is that they have been derived from measurements of the satellite instrument itself. For example, Koelemeijer et al. (2003) climatology for GOME and SCIAMACHY, Kleipool et al. (2008) for OMI and Tilstra et al. (2017) for GOME-2 and SCIAMACHY. In constructing these climatologies, it is assumed that the surface reflectance is fully isotropic, and the angular dependence of reflected light is neglected. In the minimum-LER method, surface LER values are the 1% cumulative values retrieved from the histogram of Earth reflectance over a specific scene in a climatological period. The presence of clouds increases TOA reflectance compared to clear-sky scenes, therefore taking the minimum LER assures that the surface LER values represent mostly cloud-free scenes. However, if for particular viewing and illumination geometries, the TOA reflectance appears brighter, then those measurements will not be included in the climatology. This will introduce an intrinsic (but not explicit) viewing angle dependency in the surface LER climatologies derived from the satellites. That measurements taken under different viewing geometry configurations are used to create the climatologies, does not mean that climatological surface LER values are representative for typical or average viewing geometries of the instruments.

Figure 1a, b show the minimum surface LER climatology (2007-2013) at 494 nm and 772 nm for March over Amazonia for GOME-2 onboard MetOp-A (hereafter GOME-2A) from Tilstra et al. (2017). This climatology was derived from the 1% cumulative reflectances gathered irrespective of viewing geometry. Figure 1c, d show the directional dependence of the minimum surface LER climatologies derived using the same GOME-2A measurements, but now discriminating between different geometries. For this purpose, the 24 measurements in 24 different viewing directions along the GOME-2 swath are considered independently, and then the minimum LER method is applied for each viewing direction as in the derivation of the original full swath climatology. We consider East as the 8 most eastward measurements, Nadir as the centered ones and West as the 8 most westward measurements. The average relative azimuth angle (RAA) characterizes the light scattering regime for measurements in each region: low RAA in the East (RAA = 16°) corresponds to forward scattering and high RAA (RAA = 164°) in the West corresponds to backward scattering.

In Figs. 1c, d the horizontal line is the original surface LER value obtained using all GOME-2A measurements over Amazonia, and corresponds to the average value over the box in Fig. 1a, b ($\overline{A_{\mathrm{LER}}}$ = 0.028 at 494 nm and $\overline{A_{\mathrm{LER}}}$ = 0.21 at 758 nm). The albedo is lower at 494 nm because of absorption of light by chlorophyll. At 758 nm, if only measurements of the eastern part

(E) of the orbit are used to construct the climatology, the average surface LER value is slightly lower ($\overline{A_{\mathrm{LER}}}$ = 0.19) than the value using all measurements. If only nadir (N) measurements are used, the average surface LER increases ($\overline{A_{\mathrm{LER}}}$ = 0.24), and for the westernmost measurements (W), the average surface LER increases to almost twice the original value ($\overline{A_{\mathrm{LER}}}$ = 0.37). Using the full swath climatology thus implies a slight overestimation of the surface reflectance for the eastern measurements and a strong underestimation for nadir and western measurements. This systematic effect is a consequence of the directional signature of the surface reflectance. In the backward scattering direction, canopy surfaces generally appear brighter than in the forward scatter direction (e.g. Camacho-de Coca et al. (2004)). This effect is strongest in the near-infrared (NIR, 0.7 - 2.5 μm) spectral range where the atmosphere is more transparent, and over vegetation, which has non-isotropic elements (e.g. dense trees with heterogeneous leave orientation and shadowing effects). The effect in the surface LER climatologies also appears over non-vegetated regions and at shorter wavelengths. However, it is not as strong because stronger Rayleigh scattering tends to smooth out the sensitivity to surface effects and because land surfaces are darker at shorter wavelenghts. Non-vegetated areas are usually more isotropic than vegetated areas. Because these biased surface LER climatologies are used in cloud retrievals (e.g. FRESCO Wang et al. (2008), ~~O2-O2~~ O_2-O_2 Veefkind et al. (2016)), we anticipate a substantial effect on the retrieved cloud properties and as a consequence on trace gas column retrievals that use cloud parameters retrieved in the NIR, where sensitivity to surface anisotropy is strong (such as GOME-2).

Indeed, we find that cloud fractions retrieved with FRESCO cloud retrieval from GOME-2 measurements are affected by the across-track bias in the surface LER climatology. FRESCO retrieves cloud properties in the O_2 A-band near 760 nm. Figure 2a shows that over Amazonia (in March 2008) FRESCO cloud fractions are generally lower for the eastern measurements than for nadir and western measurements. This dependency can be explained by the directional biases in the surface LER (Fig. 1d). In the nadir and west measurements, the surface LER is underestimated and the retrieval compensates this overestimating cloud fractions in order to match observed TOA reflectances. This results in higher mean effective cloud fractions for the nadir ($\overline{c_{\mathrm{eff}}}$ = 0.50) and west ($\overline{c_{\mathrm{eff}}}$ = 0.66) measurements compared to the east measurements ($\overline{c_{\mathrm{eff}}}$ = 0.33). The East - West bias ($100 \cdot (\overline{c_{\mathrm{eff,W}}} - \overline{c_{\mathrm{eff,E}}})/\overline{c_{\mathrm{eff,W}}}$) in the cloud fraction depends on the time of the year and the location. It is not only present over ~~vegetated~~ forested areas (i.e. Amazonia (50%), Equatorial Africa (42%) in March 2008) but also occurs over other regions (e.g. over Europe (25%) and Asia (10%), not shown). Furthermore, in the ensemble of western measurements in most of the regions there are very few cloud fraction values lower than 0.2. This directly impacts trace gas retrievals, because a cloud fraction of 0.2 is often used as a threshold above which it is considered difficult to retrieve tropospheric NO_2 columns (cloud screening effect). This bias in FRESCO cloud fractions is significantly higher than the cloud fraction retrieval uncertainty estimates of 0.05 due to surface albedo uncertainty (Koelemeijer et al., 2002), which underlines the need to correct for surface BRDF effects in cloud retrievals in the ~~O2-A~~ O_2-A band.

The OMCLDO2 cloud retrieval from the OMI retrieves cloud properties in the ~~O2-O2~~ O_2-O_2 band around 470 nm and uses the Kleipool et al. (2008) surface LER climatology, which is based on the same principles as the climatology used in FRESCO. Cloud fractions from the OMI instrument retrieved with the OMCLDO2 algorithm also show a West - East[1] bias (Fig. 2b) over

[1]OMI swath is divided into 60 different viewing directions; East corresponds to the 20 easternmost measurements and West to the 20 westernmost measurements

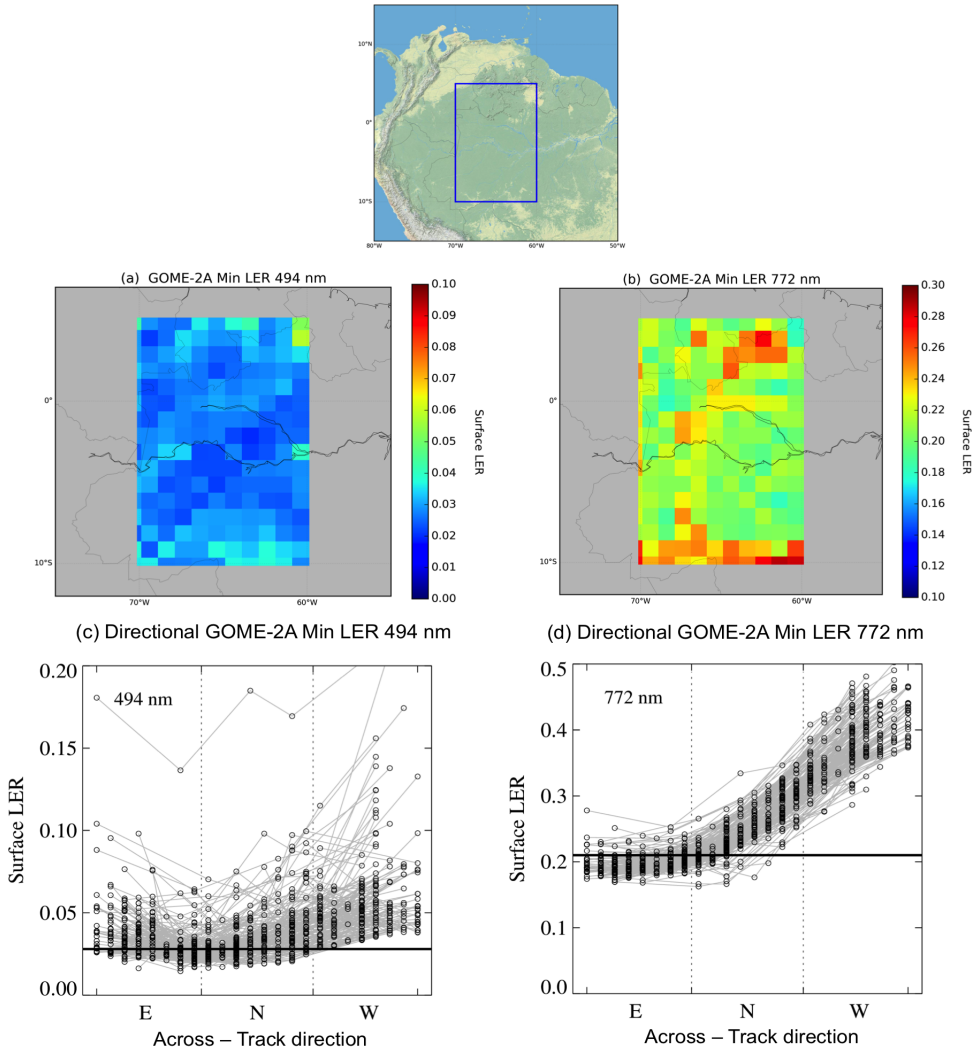

Figure 1. (a, b) Map of GOME-2A minimum surface LER climatology (2007-2013) for March at (a) 494 nm and (b) at 772 nm over Amazonia (Lat: 5N-10S, Lon: 60-70W, upper panel) at 1° x 1° resolution. (c, d) Directional dependence of surface LER climatology (2007-2013) derived from individual measurements along the swath: East (E) for the 8 easternmost pixels, Nadir (N) for the 8 center pixels and West (W) for the 8 westernmost pixels. The horizontal line represents the surface LER using the full swath which is the average of the surface LER in panels (a, b).

Amazonia (September 2005) of 26% ($\overline{c_{\mathrm{eff,W}}}$ = 0.31, $\overline{c_{\mathrm{eff,E}}}$ = 0.42) and around 15% over other regions. The effect is weaker than for GOME-2A (50% vs. 26% over Amazonia), but still substantial. The bias shown here is slightly higher than the cloud fraction retrieval uncertainty estimate which is always below 0.1 (Acarreta et al., 2004), suggesting that the bias in the ~~O2-O2~~

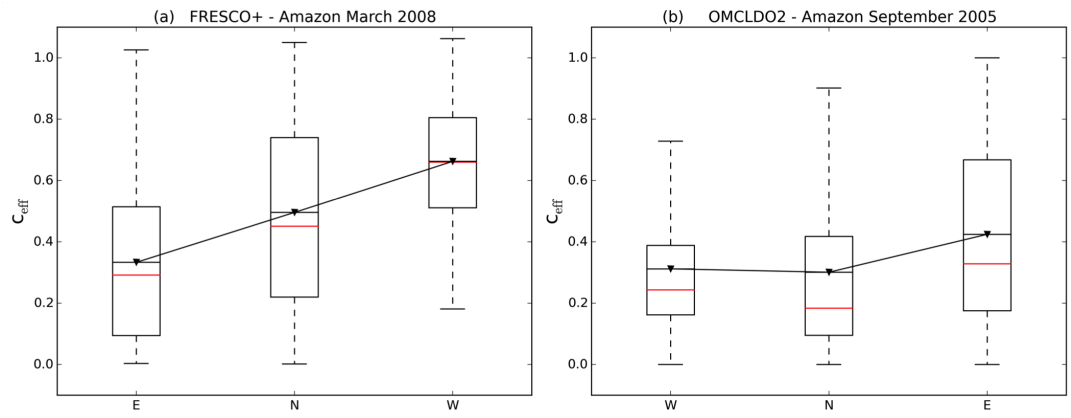

Figure 2. Box-plot of cloud fractions retrieved with (a) FRESCO cloud retrieval for GOME-2A for March 2008 and (b) OMCLDO2 cloud retrieval for OMI for September 2005 for East- Nadir- West measurements over Amazonia (Lat:5N-10S, Lon:60-70W). Black triangles correspond to mean values, red lines to median. The box represents 25th and 75th percentiles and the dashed lines the minimum and maximum values.

O_2-O_2 retrieved cloud fractions can be significant depending on location and time of the year. Because OMI angles are larger than for GOME-2, a larger effect could be expected if also the ~~O2-A~~ O_2-A band would have been used to retrieve clouds from OMI measurements.

We have shown that surface BRDF effects results in a distinct across-track bias in surface LER climatologies and cloud fractions retrieved from satellite instruments and that the effect is highly relevant in the NIR and in the visible. Errors in cloud fraction and surface albedo are the most important source of tropospheric AMF errors (Boersma et al., 2004), so we expect a strong impact on tropospheric NO_2 retrievals. In the following section we describe how to account for surface anisotropy in the radiative transfer model DAK. Then, we study how cloud retrievals and NO_2 retrievals are affected by the assumption of a Lambertian surface as compared to a realistic anisotropically reflecting surface.

3 Reflectance simulations with surface BRDF in DAK

3.1 Definition of BRDF

The amount of radiation reflected by a surface in a certain direction depends on the direction of the incident irradiance and on the direction in which the reflected radiance is observed. The surface Bidirectional Reflectance Distribution Function (BRDF) is a function that characterizes the directional reflecting properties of a surface. The surface BRDF mathematically describes the angular distribution of the surface reflectance: R_{g} as a function of the illumination direction (incident, θ', φ') and viewing direction (reflected, θ, φ) (see Fig. 3). It is expressed as the ratio of the reflected radiance in a certain direction (dL) and the

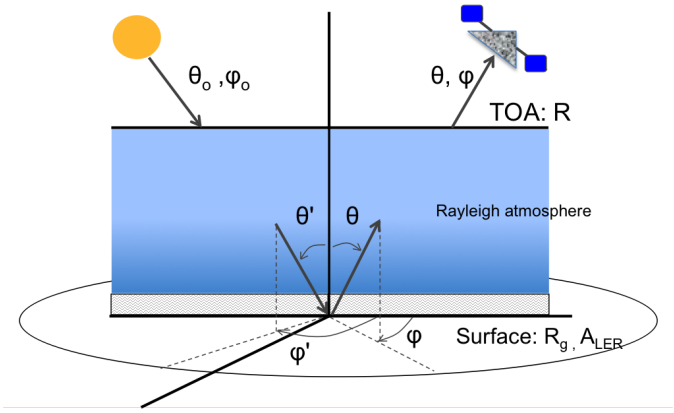

Figure 3. Sketch of the surface to top-of-atmosphere system with zenith and azimuth angles that define incident (θ', φ') and reflected (θ, φ) directions of light. Direct incident solar light is described by (θ_0, φ_0). A_{LER} is the Lambertian surface albedo and R_{g} the surface BRDF.

incident irradiance from a particular direction ($\mathrm{d}E'$) (Nicodemus et al., 1992):

$$R_{\mathrm{g}}(\theta', \varphi'; \theta, \varphi) = \mathrm{d}L(\theta', \varphi'; \theta, \varphi)/\mathrm{d}E'(\theta', \varphi'). \tag{1}$$

The zenith angle (θ) and the azimuth angle (φ) define the direction of incidence (θ', φ') and reflectance (θ, φ), as sketched in Fig. 3.

The albedo of a surface is generally defined as the ratio of the irradiance reflected by a surface area into the whole hemisphere and the irradiance incident to the surface with hemispherical angular extent (i.e. coming from all directions) (Schaepman-Strub et al., 2006). For particular illumination and viewing conditions, black-sky and white-sky albedo are defined, and they are obtained through hemispherical integration of the surface BRDF. The black-sky albedo is the albedo without diffuse component in the incident irradiance, i.e. the illumination of the surface is from a single direction. It is defined as the integral of the BRDF over the reflection hemisphere of 2π steradians (directional-hemispherical reflectance):

$$A_{\mathrm{bs}}(\theta', \lambda) = \int_{2\pi} \int_{\frac{\pi}{2}} R_{\mathrm{g}}(\theta', \varphi'; \theta, \varphi) \cos\theta \sin\theta \mathrm{d}\theta \mathrm{d}\varphi. \tag{2}$$

In the particular case when there is only a diffuse isotropic component in the incident flux, the white-sky albedo can be defined as the integral of the surface BRDF over both the incident and reflection hemispheres (bi-hemispherical reflectance):

$$A_{\mathrm{ws}}(\lambda) = \int_{2\pi} \int_{\frac{\pi}{2}} \int_{2\pi} \int_{\frac{\pi}{2}} R_{\mathrm{g}}(\theta', \varphi'; \theta, \varphi) \cos\theta' \sin\theta' \cos\theta \sin\theta \mathrm{d}\theta \mathrm{d}\varphi \mathrm{d}\theta' \mathrm{d}\varphi'. \tag{3}$$

The so-called blue-sky albedo is a linear combination of A_{bs} and A_{ws} weighted by the fraction of diffuse skylight. The use of either A_{bs}, A_{ws} or A_{LER} in different applications depends on the assumptions of each parameter and the particular application. In the NIR, the diffuse component in the radiation field is much smaller than the direct component so the use of the A_{bs} is

justified because it assumes only direct light. A_{ws} might be more suitable for applications in the UV/visible spectral range where the diffuse component of the incident light may be of comparable size as the direct component. In any case, MODIS visible and NIR A_{ws} and A_{bs} do not differ on average more than 5% in summer (Oleson et al., 2003). A_{ws} is constant with SZA, so its use is valid as a A_{LER} but it accounts for some surface BRDF effects (Eq. 3).

Several models have been developed to describe surface BRDF (Wanner et al., 1995). These are either physical, empirical or semi-empirical models. Physical models are constructed using laws of physics to explicitly describe the processes that lead to the anisotropic behaviour of surface reflectance. Empirical models characterize the BRDF using mathematical functions that are suitable to describe the observed surface reflectance. Semi-empirical models describe the surface BRDF as a weighted sum of empirical functions derived from physical approximations.

Semi-empirical models are commonly used for global surface BRDF characterization using remote sensing instruments. In these models, surface reflectance is represented as linear combination of different terms (the so-called kernels) that characterize different types of scattering that lead to the directional signatures on the reflectance (Roujean et al., 1992). Typically these terms consist of an isotropic term, a volume scattering term, and a geometric scattering term. The weights of the kernels cannot be directly interpreted as physical characteristics from the reflecting surface, but just as a first order approximation of the structure of the surface BRDF (Gao et al., 2003).

In the semi-empirical BRDF Ross Thick-Li Sparse (hereinafter Ross-Li) kernel-driven model, the surface reflectance is expressed as a sum of an isotropic term and two kernels (K_{i}) that depend on incident zenith angle (θ'), viewing zenith angle (θ) and relative azimuth angle ($\varphi - \varphi'$):

$$R_{\mathrm{g}}(\theta,\theta',\varphi-\varphi',\lambda) = f_{\mathrm{iso}}(\lambda) + f_{\mathrm{vol}}(\lambda)K_{\mathrm{vol}}(\theta,\theta',\varphi-\varphi') + f_{\mathrm{geo}}(\lambda)K_{\mathrm{geo}}(\theta,\theta',\varphi-\varphi'). \quad (4)$$

In Eq. 4 K_{i} are the kernels from the semi-empirical Ross-Li model that describe the three basic scattering types and f_{i} are the surface BRDF parameters that are retrieved from surface reflectance observations from satellite measurements (e.g. MODIS). The surface reflectance cloud-free observations used to obtain the surface BRDF parameters are corrected for absorption and scattering by atmospheric gases, aerosols and thin clouds (Vermote et al., 1997). Improvements in the atmospheric correction scheme include as much information as possible derived from the satellite itself (e.g. MODIS aerosol optical thickness) (Vermote and Kotchenova (2008)).

The isotropy parameter (f_{iso}) represents the isotropic scattering from a nadir incident and nadir view position. The volumetric scattering is represented by the Ross-Thick kernel, K_{vol}. It is derived in a single scattering approximation from radiative transfer theory for a thick homogeneous layer of small scatterers, with equal reflectance and transmittance (Roujean et al., 1992). To account for the reflectance peak in the backscatter direction (i.e. the hot-spot effect) we include the modification on the volumetric kernel by Maignan et al. (2004). The geometric scattering is represented by the Li-Sparse kernel, K_{geo}. For this case, the scene is assumed to contain sparse objects that cast perfectly black shadows with sunlit and shaded portions of the ground and crown contributing to the modelled reflectance of the scene (Li and Strahler, 1986). The exact formulae for these kernels are summarized in Appendix A.

3.2 Surface BRDF implementation in DAK

The radiative transfer model DAK (Doubling-Adding KNMI, Lorente et al. (2017), Stammes et al. (1989), de Haan et al. (1987)) is used in the GOME-2 and OMI cloud retrievals (FRESCO and OMCLDO2) and in the DOMINO NO_2 retrieval. Originally DAK only considered Lambertian surfaces. To account for the surface reflectance anisotropy in DAK, we have implemented the Ross-Li kernel-driven model. We chose this model for consistency with the retrieval algorithm of the MODIS BRDF/Albedo product that we will use in our simulations. The MODIS satellite provides a reliable surface BRDF product and its resolution is suitable to capture surface anisotropy variations for OMI and GOME-2 resolution. MODIS BRDF/Albedo products have been successfully used in different fields of atmospheric and climate science such as analysis of radiative forcing due to vegetation change (Myhre et al., 2005) and assessment of land surface albedo in global climate models (Oleson et al., 2003).

After the implementation of the Ross-Li surface BRDF model in DAK, the surface reflectance matrix R_{g} now contains the full reflection properties of the surface and substitutes the constant isotropic value used for the Lambertian case. This matrix is filled with the surface reflectance calculated with the Ross-Li BRDF model via Eq. 4 as a function of θ, θ' for a specific $\varphi - \varphi'$. For the Lambertian case, the matrix only contains the (1,1) element, which is the value of the surface albedo. We neglect polarization in the BRDF. In the Doubling-Adding method for radiative transfer calculation, all the matrices (scattering, reflection and transmission matrices) are expanded in Fourier series for the integration over $\varphi - \varphi'$ following the approach in de Haan et al. (1987). For each Fourier term the Doubling-Adding procedure is applied separately, including the addition of the surface. The m-th Fourier coefficient matrix for the surface reflectance matrix is obtained from the relation:

$$R_{\mathrm{g}}^{m}(\mu, \mu') = \frac{1}{2\pi} \int_{0}^{2\pi} d(\varphi - \varphi') \cos m(\varphi - \varphi') R_{\mathrm{g}}(\mu, \mu', \varphi - \varphi') \tag{5}$$

where μ, μ' are the cosines of the zenith angles in the scattered and incident direction (θ, θ') respectively and $\varphi - \varphi'$ is the difference between the scattered and incident azimuth angles.

The coefficients of the Fourier expansion (Eq. 5) are calculated with the Gauss-Legendre quadrature integration method. It is possible to apply this method because the surface reflection matrix R_{g} is known at a certain number of division points $\varphi - \varphi'$. The number of Fourier terms (m) and Gaussian points for azimuth ($\varphi - \varphi'$) integration needed to resolve the surface BRDF shape depends on the illumination and viewing geometry. For geometries close to the hot-spot region in the backscatter direction, the number of Fourier terms and Gaussian points needed to reproduce the original BRDF increases significantly with respect to geometries outside the hot-spot. In order to reach an accuracy of 10^{-3} (difference between the original BRDF and the reconstructed BRDF with the Fourier expansion) over the hot spot region, 720 Gaussian points are needed for the azimuth-integration, and 300 Fourier terms. Outside the hot-spot region, using 60 Gaussian points and 30 Fourier terms in DAK reproduces the original surface reflectance values with an accuracy higher than 10^{-5}. In the final implementation of the surface BRDF in the DAK RTM and in order to have an optimal simulation time, we used 100 Fourier terms and 360 Gaussian points for $\varphi - \varphi'$, also over the hot-spot. The overall accuracy obtained with these numbers is within the errors of the radiative transfer modelling for application in satellite retrievals (Lorente et al., 2017).

One of the disadvantages of empirical models is that they depend on observations to derive the parameters f_{i} that describe the surface BRDF. Kernel based semi-empirical models like the Ross-Li model implemented in DAK only describe the surface reflection accurately for the range of illumination and viewing geometries of the measurements from which they have been derived (Litvinov et al., 2011). The geometries for which the semi-empirical models are valid are thus limited by extreme geometries of instruments like MODIS, which are typically 60-70 degrees for θ and θ'. This limit overlaps well with the θ, θ' values in OMI and GOME-2 measurements for which clouds and trace gas columns are retrieved. For geometries outside the range of MODIS measurement geometries, surface reflectance variations need to be extrapolated.

In radiative transfer modelling with the Doubling-Adding method, in order to calculate the radiation field correctly, the reflectance and transmittance values are needed for all θ, θ' between 0-90 degrees to integrate over the complete hemisphere. However, after implementing the Ross-Li BRDF model in DAK, surface reflectance was negative or too high for some combinations of extreme geometries. In order to avoid these unphysical values, we tried various ways of extrapolating values from valid (MODIS-range) angles to the more extreme angles. The different methods did not affect TOA reflectance and albedo values by more than 1%. Finally, we constrained the surface reflectance to the range $[0,1]$ as in Eq. 6. This is reasonable as negative surface reflectance values are not physically valid and in nature surfaces with reflectance higher than 1 do not usually occur (expect e.g. in surfaces covered by snow or ice). Therefore,

$$\begin{aligned} &\text{If } R_{\mathrm{g}}(\mu_{\mathrm{i}}, \mu'_{\mathrm{i}}, \varphi_{\mathrm{i}} - \varphi'_{\mathrm{i}}) < 0 \quad \text{then} \quad R_{\mathrm{g}}(\mu_{\mathrm{i}}, \mu'_{\mathrm{i}}, \varphi_{\mathrm{i}} - \varphi'_{\mathrm{i}}) = 0. \\ &\text{If } R_{\mathrm{g}}(\mu_{\mathrm{i}}, \mu'_{\mathrm{i}}, \varphi_{\mathrm{i}} - \varphi'_{\mathrm{i}}) > 1 \quad \text{then} \quad R_{\mathrm{g}}(\mu_{\mathrm{i}}, \mu'_{\mathrm{i}}, \varphi_{\mathrm{i}} - \varphi'_{\mathrm{i}}) = 1. \end{aligned} \tag{6}$$

Figure 4 is an example of the surface reflectance computed with the Ross-Li BRDF model for a surface with parameters (f_{iso}, f_{vol}, f_{geo}) = (0.0399, 0.0245, 0.0072). This combination of f_{i} values are the spatially averaged parameters from MODIS (BRDF/Albedo product MCD43A1) Band 3 (459-479 nm) over Amazonia (Lat: 5N-10S, Lon: 60-70W) for March 2008. This representation of a vegetated surface will be used in all the simulations in Sect. 3. The backscatter direction corresponds to values of $\varphi - \varphi'$ = 180° in the polar plot (Fig. 4b) and negative values of θ in the principal plane plot (Fig. 4a). In the backscatter direction, the surface reflectance is two times higher than in the forward scatter direction ($\varphi - \varphi'$ = 0° in Fig. 4b and positive θ in Fig. 4a). In the backscatter direction the so-called hot-spot is clearly visible when θ = (-) 30° = θ'.

The surface reflectance dependence on geometry as shown in Fig. 4 does not exist when a constant isotropic albedo or surface LER is used. Using a constant albedo for this surface of 0.03 (the equivalent A_{ws} is 0.034) means that in the backscatter direction the surface reflectance is underestimated. On the contrary, in the forward direction the surface reflectance is overestimated if an isotropic surface albedo is used. This surface reflectance difference between forward-backward scattering direction thus qualitatively explains the East-West bias in the surface LER in Fig. 1. West measurements in GOME-2 correspond to the backscatter direction, and for this direction the surface reflectance is higher than in the forward scatter direction, i.e. East measurement in GOME-2. How this affects retrieved effective cloud fractions and NO_2 AMFs from GOME-2 and OMI will be analysed in Sect. 4.

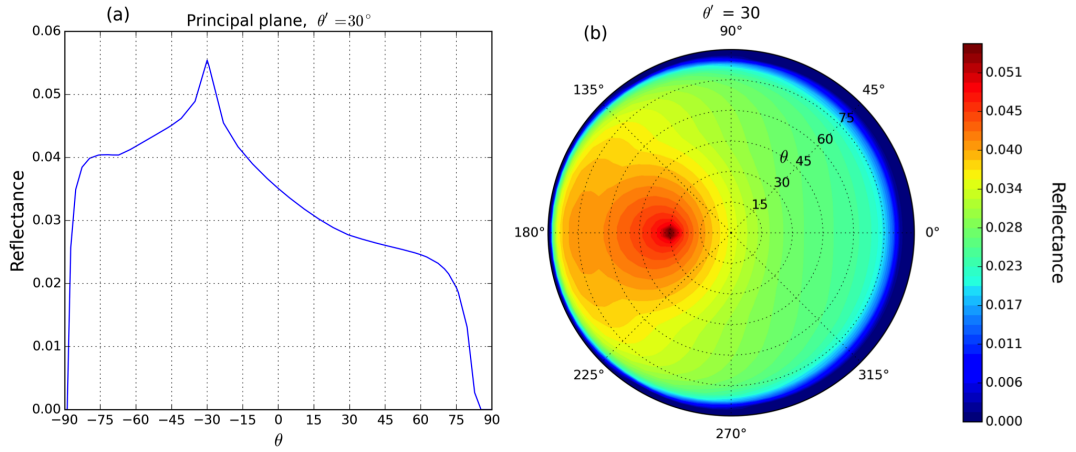

Figure 4. Surface reflectance modelled with the Ross-Li surface BRDF model with parameters from MODIS band 3 (459-479 nm) representing a vegetated surface over Amazonia (a) as function of viewing zenith angle in the principal plane ($\varphi - \varphi' = 180^\circ$ for negative θ and $\varphi - \varphi' = 0^\circ$ for positive θ) and (b) in a polar plot with $\varphi - \varphi'$ along the azimuth axis and θ along the polar axis, for $\theta' = 30^\circ$.

3.3 Evaluation of surface BRDF effects in DAK TOA reflectances

To evaluate the surface BRDF implementation in DAK we compare TOA reflectances with those simulated by other state-of-the-art radiative transfer models that include a description of surface BRDF effects. Both SCIATRAN (Rozanov et al., 2014) and LIDORT (Spurr, 2004) model the surface reflectance using the Ross-Li model. To minimize the differences due to factors other than the surface BRDF implementations itself, the settings of the three RTMs were as similar as possible. These settings include: no polarization, a plane parallel standard mid-latitude atmosphere and absorption by O_3, O_2-O_2 and NO_2. We select two combinations of the Ross-Li BRDF parameters to model surface reflectance of different surfaces. We simulate TOA reflectances at two different wavelengths: 469 and 645 nm. These wavelengths correspond to the middle of the MODIS band 3 (459-479 nm) and band 1 (620-670 nm), respectively.

Figure 5 shows the simulated TOA reflectance by DAK, SCIATRAN and LIDORT as a function of VZA along the principal plane at 469 nm and 645 nm. The agreement between the models is within 0.5% for geometries outside the hot-spot region, and DAK and SCIATRAN agree within 1% over the hot-spot. With this simple validation we assure that our surface BRDF implementation in DAK is correct. The viewing geometry dependency of the TOA reflectance is the effect of Rayleigh scattering of a clean atmosphere. By comparing Fig. 4a with Fig. 5 we see that the effect of surface reflectance anisotropy is dampened by the scattering in the atmosphere but the hot-spot effect is still visible at both wavelengths after the radiation has passed through the atmosphere. Figure 5 also shows that the hot-spot effect is less prominent in TOA reflectance at 469 nm compared to 645 nm, where the atmosphere is more transparent. At 469 nm Rayleigh scattering is stronger than at 645 nm, reducing the effects of surface anisotropy on the TOA reflectance.

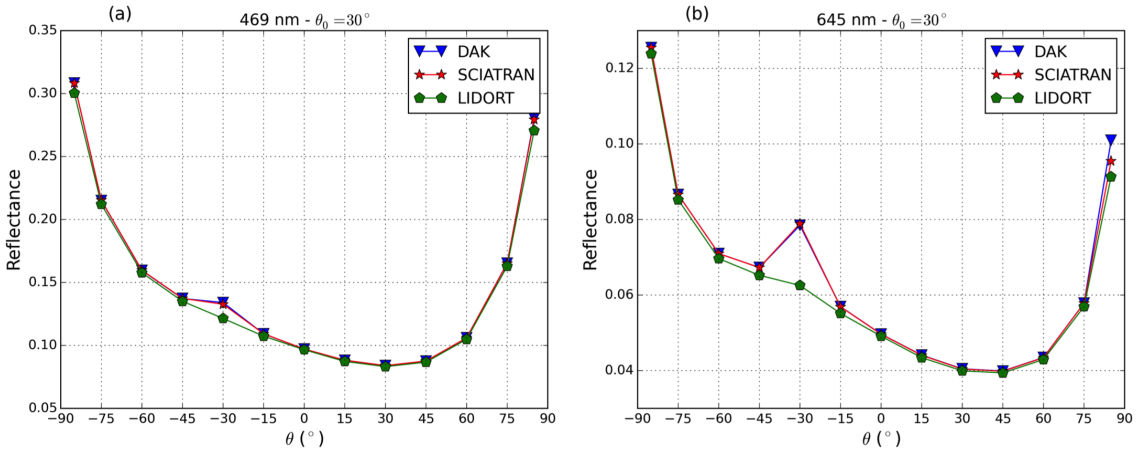

Figure 5. TOA reflectance at (a) 469 nm and (b) 645 nm simulated by DAK (blue), SCIATRAN (red) and LIDORT (green) with the Ross-Li surface BRDF model with parameters representing a vegetated surface over Amazonia as in Fig.4 as a function of the viewing zenith angle in the principal plane ($\varphi - \varphi_0 = 180°$ for negative θ and $\varphi - \varphi_0 = 0°$ for positive θ), for $\theta_0 = 30°$.

We now compare TOA reflectance simulated with surface BRDF and TOA reflectance simulated assuming a Lambertian surface at 469 nm (Fig. 6a, b) and 758 nm (Fig. 6c, d). For simulations at 758 nm we use surface BRDF parameters from MODIS band 2 (841-876 nm) to account for the increase in surface reflectivity near 700 nm (the so-called red edge, e.g.Tilstra et al. (2017)). To test the representativeness of band 2 at 758 nm, we scaled the parameters from band 3 (459-479 nm) using the ratio of reflectance at 772 nm and 469 nm, and the differences with the parameters from MODIS band 2 were negligible. For the Lambertian case, we use the equivalent $A_{\rm ws}$ calculated using the surface BRDF model with Eq. 3. Figure 6b shows that at 469 nm, the highest absolute differences are around the hot-spot region in the backward scattering direction, where TOA reflectance with BRDF is up to 15% higher than the TOA reflectance for the Lambertian case. In the forward scatter direction, TOA reflectance with surface BRDF is 7% lower than for the Lambertian surface. At 758 nm the effect of surface reflectance anisotropy is much stronger than at 469 nm (Fig. 6c). The highest absolute differences at 758 nm (Fig. 6d) are in the hot-spot region in the backscatter direction (up to 30%) and for very extreme angles ($\theta > 85°$) in the forward scattering direction.

These results are consistent with those shown in Fig. 1 and Fig. 2: for GOME-2A West measurements (backscatter direction), TOA reflectances with surface BRDF are higher than for the Lambertian surface. If these differences are not accounted for in the cloud retrieval, cloud fractions will be biased high in the West measurements to match the measured TOA reflectance. For East measurements in the forward scatter direction, TOA reflectance with surface BRDF is lower than for the Lambertian surface. Cloud fractions retrieved with surface LER will be biased low to match the measured TOA reflectance. Results from Fig. 6 underline that surface BRDF effects in retrieved cloud fractions are stronger for FRESCO at 758 nm than for OMCLDO2 at 477 nm. Our results also show that the error in TOA reflectances due to the use of a Lambertian albedo is substantial, but its

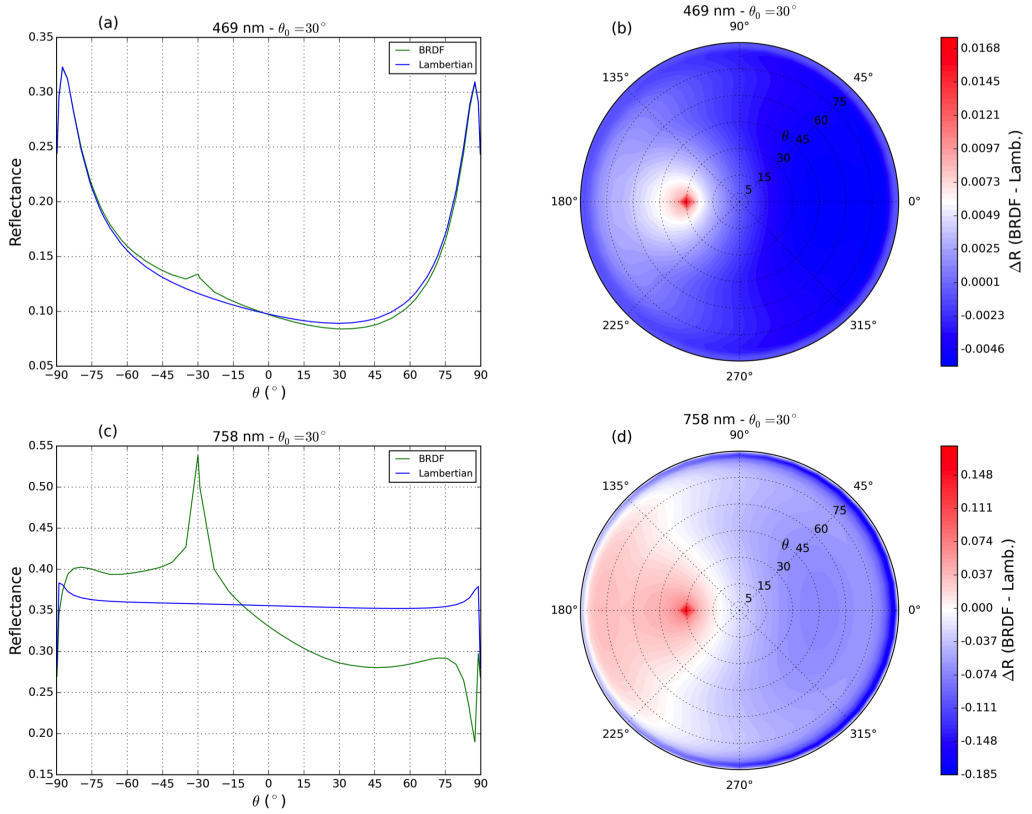

Figure 6. (a, c) TOA reflectance as a function of viewing zenith angle simulated by DAK at 469 nm and 758 nm with a Lambertian surface (blue line) and with surface BRDF (green line) in the principal plane ($\varphi - \varphi_0$ = 180° for negative θ and $\varphi - \varphi_0$ = 0° for positive θ). (b, d) Absolute differences between TOA reflectance with surface BRDF and with a Lambertian surface at 469 nm and 758 nm. Surface BRDF parameters represent a vegetated surface over Amazonia at 469 nm (f_{iso}, f_{vol}, f_{geo}) = (0.0399, 0.0245, 0.0072) and 758 nm (f_{iso}, f_{vol}, f_{geo}) = (0.36, 0.24,0.03). Note the different scales.

magnitude is highly dependent on the spectral and geometrical characteristics of the measurements: effects are stronger at 758 nm and around the hot-spot region in the backscatter direction.

4 Role of surface BRDF in cloud retrievals

4.1 Synthetic cloud fraction retrieval

In Sect. 2 we showed that there is an East-West bias in the retrieved cloud fractions from GOME-2 and OMI. Effective cloud fractions in FRESCO and OMCLDO2 are retrieved as follows (Stammes et al. (2008),Veefkind et al. (2016)):

$$c_{\mathrm{eff}} = \frac{R_{\mathrm{meas}} - R_{\mathrm{cr}}}{R_{\mathrm{cd}} - R_{\mathrm{cr}}}. \tag{7}$$

R_{meas} is the TOA reflectance measured by the satellite instrument, R_{cr} is the simulated clear-sky TOA reflectance, and R_{cd} is the simulated cloudy-sky TOA reflectance assuming that the cloud is a Lambertian reflector with a fixed albedo of 0.8. In the current versions of FRESCO (v7) and OMCLDO2 (v2.0) cloud retrievals, the simulated clear-sky TOA reflectances in Eq. 7 assume that the surface is Lambertian. Due to this assumption, any surface anisotropy signal is neglected in the measured TOA reflectance (R_{meas}), and, consequently in the retrieved effective cloud fraction.

To improve our understanding of how surface reflectance anisotropy influences the retrieval of cloud fractions, we use the forward model DAK to approximate R_{meas} ~~with DAK~~ by simulating the TOA reflectance for a scene with a Henyey-Greenstein cloud and surface reflectance anisotropy. This resembles what the satellite would measure in ~~the presence of a scattering cloud~~a realistic cloudy scene. We express R_{meas} as the sum of TOA reflectance of the cloudy and the clear parts of the scene, weighted by a geometric cloud fraction c_{geo} (independent pixel approximation):

$$R_{\mathrm{meas}} \approx R_{\mathrm{sim}} = c_{\mathrm{geo}} \cdot R_{\mathrm{cd}} + (1 - c_{\mathrm{geo}}) R_{\mathrm{cr}}. \tag{8}$$

The settings of the simulations are summarized in Table 1. We simulate TOA reflectances and cloud fractions in the spectral regions where cloud fractions are calculated in the cloud algorithms. The Ross-Li BRDF parameters are from a climatology created by the QA4ECV Land Group at the Mullard Space Science Laboratory (University College London). This dataset consists of daily BRDF parameters collected from 16 years of MODIS measurements (Strahler et al. (1999), MCD43A1) from 2000 to 2016 (QA4ECV-WP4, 2016). Parameters from band 3 (459 - 479 nm) are representative for simulations in the ~~O2-O2~~ O_2-O_2 absorption band and parameters from band 2 (841-876 nm) for simulations in the ~~O2-A~~ O_2-A band (see Sect. 3.2). Monthly averaged parameters from this dataset over Amazonia are shown in Fig. S2,3 in the supplementary material.

We calculate retrieved cloud fractions using Eq. 7 with R_{cr} simulated with a Lambertian surface consistent with the current ~~O2-O2~~ O_2-O_2 and FRESCO+ retrievals (hereafter Lambertian c_{eff}) and by accounting for surface BRDF effects (hereafter BRDF c_{eff}). The Lambertian cloud is located at the same pressure level as the Henyey-Greenstein cloud so we can isolate surface BRDF effecst on cloud fraction only (see settings in Table 1).

Figure 7 shows that cloud fractions accounting for surface BRDF effects (dashed lines) depend only weakly on geometry whereas cloud fractions with a Lambertian surface (solid lines) are higher in the backward scattering direction, at both 477 nm and 758 nm and especially for the lowest c_{geo}. At 758 nm this is true even for a geometric cloud fraction as high as 0.5. In the backward scattering direction, surface reflectance is higher than reflectance by a Lambertian surface. Therefore clear-sky

Table 1. Settings for Lambertian and BRDF $c_{\rm eff}$ simulations in Sect. 4.1. Inverse model for Lambertian $c_{\rm eff}$ reproduces current O_2-O_2 and FRESCO+ retrievals, with Lambertian surface and Lambertian cloud. Inverse model for BRDF $c_{\rm eff}$ reproduces the retrieval accounting for surface BRDF effects.

Forward model, $R_{\rm meas}$		**Inverse model**, $c_{\rm eff}$	
Henyey-Greenstein scattering cloud		**Lambertian cloud** ($R_{\rm cd}$)	
Asymmetry parameter, g	0.85	Cloud albedo, $A_{\rm cd}$	0.8
Cloud optical thickness, τ_c	30	Cloud altitude	1-2 km
Cloud altitude	1-2 km	**Lambertian $c_{\rm eff}$: surface albedo ($A_{\rm ws}$) for** $R_{\rm cr}$	
Geometric cloud fraction, $c_{\rm geo}$	0, 0.05, 0.2, 0.5	λ = 477 nm	0.0217
Surface reflectance: BRDF parameters ($f_{\rm iso}$, $f_{\rm vol}$, $f_{\rm geo}$) for $R_{\rm cr}$		λ = 758 nm	0.337
λ = 477 nm	0.03, 0.02, 0.01	**BRDF $c_{\rm eff}$: surface parameters ($f_{\rm iso}$, $f_{\rm vol}$, $f_{\rm geo}$) for** $R_{\rm cr}$	
λ = 758 nm	0.4, 0.25, 0.08	λ = 477 nm	0.03, 0.02, 0.01
		λ = 758 nm	0.4, 0.25, 0.08

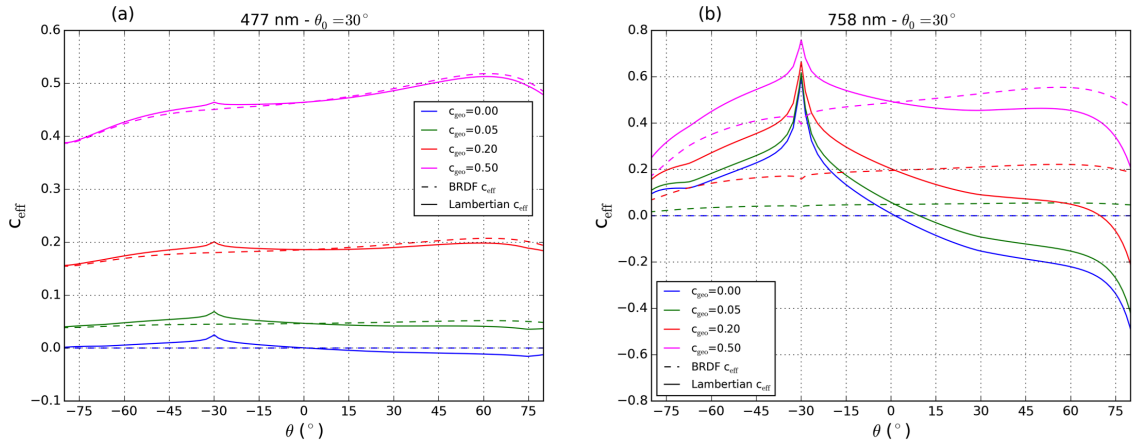

Figure 7. Simulated effective cloud fraction at (a) 477 nm and (b) 758 nm as a function of viewing zenith angle for different geometric cloud fractions along the principal plane ($\varphi - \varphi_0$ = 180° for negative θ and $\varphi - \varphi_0$ = 0° for positive θ). θ_0 = 30° and $c_{\rm geo}$ = 0, 0.05, 0.2 and 0.5. At 477 nm: BRDF parameters (solid line) ($f_{\rm iso}$, $f_{\rm vol}$, $f_{\rm geo}$) = (0.03, 0.02, 0.01) and for Lambertian surface $A_{\rm ws}$ = 0.0217 (dashed line). At 758 nm: BRDF parameters (solid line) ($f_{\rm iso}$, $f_{\rm vol}$, $f_{\rm geo}$) = (0.4, 0.25, 0.08) and for Lambertian surface $A_{\rm ws}$ = 0.337 (dashed line).

TOA reflectance with a Lambertian surface cannot explain the higher simulated reflectance in Eq. 7, which results in high Lambertian $c_{\rm eff}$.

Surface BRDF effects are more important for small cloud fractions, and less for large cloud fractions. For cloudy pixels the effect of surface reflectance anisotropy vanishes because the scattering by the cloud dominates in the measured reflectance. Fig.

7 shows that for large c_{geo}, the viewing zenith angle dependency of the effective cloud fractions is due to the Henyey-Greenstein scattering cloud, which gives relatively higher scattering in the forward direction.

At 477 nm, surface BRDF effects on cloud fractions are less evident than at 758 nm. In the visible spectral region, surface BRDF effects are suppressed by Rayleigh scattering smoothing out the surface anisotropy effects on TOA reflectances. For lower geometric cloud fraction, Lambertian cloud fractions are moderately higher (by 0.05) in the backscatter direction than in the forward scatter direction. These findings underscore the relevance of accounting for surface BRDF effects because measurements with small cloud fractions are most sensitive to pollution in the lower troposphere.

Differences in Lambertian cloud fractions between backward and forward scattering directions at 758 nm are on average 0.35. At 477 nm, the differences amount to 0.1, depending on the surface and the geometry. This is consistent with the observed bias in FRESCO and OMCLDO2 cloud fractions shown in Fig. 2. The absence of a backward-forward scattering dependency in the BRDF c_{eff} implies that accounting for surface BRDF effects will reduce the East-West across-track bias in retrieved cloud fractions.

4.2 GOME-2A cloud fraction simulations

We simulate Lambertian and BRDF cloud fractions for GOME-2A measurements over Amazonia in March 2008. We use the exact illumination and viewing geometry $(\theta, \theta_0, \varphi - \varphi_0)$ of each individual measurement and colocate MODIS pixels with the GOME-2A pixel centre to obtain the surface BRDF parameters over the scene. For Lambertian cloud fractions, we use the GOME-2A surface LER value from Tilstra et al. (2017). To simulate the measured reflectance, we assume ~~the~~ a geometric cloud fraction distribution ~~shown in Fig. 8a for East measurements and the distribution in Fig. 8d for West measurements. The~~ with an area-wide average ~~cloud fraction of these distributions is~~ of $\overline{c_{\mathrm{geo}}} = 0.33$. Figure 8a,d show the $\overline{c_{\mathrm{geo}}}$ distribtuion for East and West measurements respectively.

Figure 8 shows simulated Lambertian (b,e) and BRDF (c,f) effective cloud fractions for East and West GOME-2A measurements. For East measurements, both Lambertian ($\overline{c_{\mathrm{eff}}} = 0.32$) and BRDF ($\overline{c_{\mathrm{eff}}} = 0.28$) cloud fraction simulations capture the original geometric cloud fraction distribution and absolute values. This means that surface BRDF effects are weaker in the East, consistent with the smaller surface LER climatology bias for measurements on the East part of the orbit (Fig. 1). For West measurements, the original distribution is reproduced well in the BRDF cloud fractions ($\overline{c_{\mathrm{eff}}} = 0.29$), but the Lambertian values show a significant overestimation ($\overline{c_{\mathrm{eff}}} = 0.51$). A box-plot of these distributions is shown in Fig. S4 in the supplementary material. The East-West bias in the Lambertian simulation (0.2) is considerably reduced (0.01) for the BRDF cloud fractions: the across-track bias in the FRESCO data is a direct consequence of neglecting surface BRDF effects. We conclude that accounting for these surface BRDF effects can largely solve the bias in cloud fractions measured in the backscatter regime.

5 Role of surface BRDF in NO_2 retrievals

Here we investigate the effects of accounting for surface reflectance anisotropy on tropospheric NO_2 column retrievals under clear-sky and partly cloudy conditions. We calculate tropospheric AMFs with surface BRDF and with a Lambertian surface,

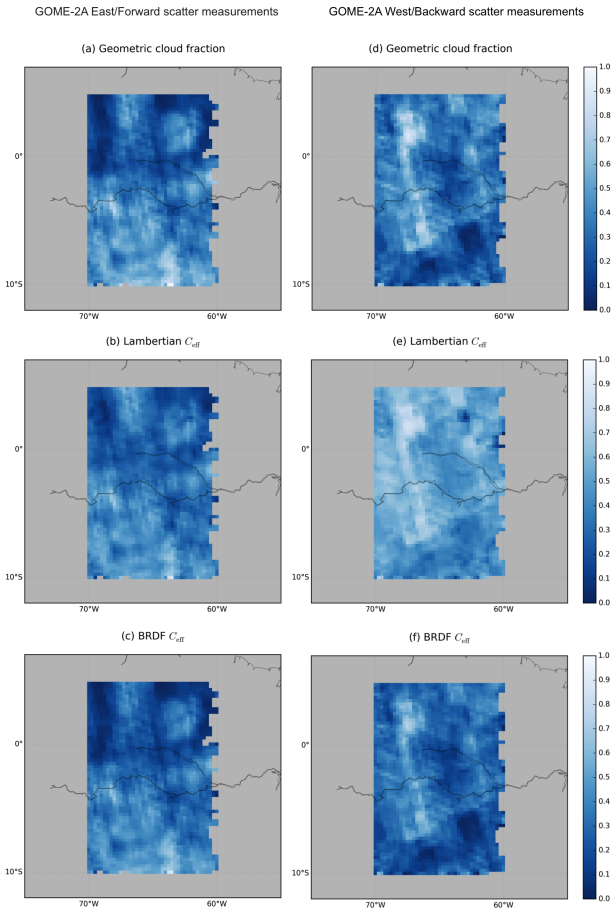

Figure 8. Geometric cloud fraction distributions for (a) East and (d) West GOME-2A measurements. (b, e) Lambertian and (c, f) BRDF cloud fraction simulations for East (first column) and West (second column) GOME-2A measurements. Plots show averaged cloud fractions in a 0.25°x0.25° grid over Amazonia (Lat: 5N-10S, Lon: 60-70W) for March 2008.

including the surface BRDF effects on retrieved cloud fractions (Sect. 4) for GOME-2A measurements over Amazonia and over France.

In satellite retrievals of trace gases, an air mass factor (M) is used to convert the slant column density (N_{s}, SCD) from the measured reflectance spectra into the vertical column density (N_{v}, VCD):

$$M(R_{\mathrm{s}}, P_{\mathrm{s}}, f_{\mathrm{cd}}, P_{\mathrm{cd}}, \overrightarrow{\mathrm{x_a}}, \theta, \theta_0, \varphi - \varphi_0) = \frac{N_{\mathrm{s}}}{N_{\mathrm{v}}}. \tag{9}$$

The AMF depends on the surface reflectance (R_{s}), surface pressure (P_{s}), cloud fraction and pressure ($f_{\mathrm{cd}}, P_{\mathrm{cd}}$), a priori NO_2 profile ($\overrightarrow{\mathrm{x_a}}$) and measurement geometry ($\theta, \theta_0, \varphi - \varphi_0$).

Here, tropospheric NO_2 AMFs are calculated by differencing the logarithm of simulated TOA reflectances with and without trace gas in the troposphere divided by the absorption optical thickness of the gas $\tau_{\rm gas}$:

$$M = -\frac{\ln R(\tau_{\rm gas}) - \ln R(\tau_{\rm gas} = 0)}{\tau_{\rm gas}}. \quad (10)$$

AMF is directly affected by the assumption of a Lambertian surface instead of an anisotropic surface in the simulated TOA reflectance. In adition, AMFs are indirectly affected by the cloud radiance fraction ($f_{\rm cd}$) used to correct for residual clouds, in which calculation a Lambertian surface is assumed as well. To account for the presence of clouds, we use the independent pixel approximation (IPA, see also Eq. 8) which consists of calculating the total AMF for a partly cloudy scene as a linear combination of cloudy ($M_{\rm cd}$) and clear ($M_{\rm cr}$) components of the AMF, weighted by the cloud radiance fraction w:

$$M = wM_{\rm cd} + (1-w)M_{\rm cr}. \quad (11)$$

The use of a Lambertian surface thus influences the AMF directly via $M_{\rm cr}$ and indirectly via w:

$$w = \frac{c_{\rm eff} R_{\rm cd}}{c_{\rm eff} R_{\rm cd} + (1 - c_{\rm eff}) R_{\rm cr}} \quad (12)$$

where $c_{\rm eff}$ is the cloud fraction and $R_{\rm cd}$, $R_{\rm cr}$ the radiances for a totally cloudy and clear-sky scene, respectively. Cloud radiance fraction depends on the Lambertian surface assumption via $R_{\rm cr}$ and $c_{\rm eff}$.

5.1 BRDF effects on tropospheric NO_2 air mass factors

We calculate AMFs with Eq. 10 by simulating TOA reflectances with surface BRDF and with a Lambertian surface. The settings of the simulations are summarized in Table 2. Based on our analysis (Sect. 4.1), we include a change of $\pm$ 0.05 over the Lambertian cloud fraction with a decrease of -0.05 in the backward scattering direction and an increase of +0.05 in the forward scattering direction, to quantify how the surface BRDF effects on clouds propagate to the final AMF.

Figure 9a shows surface BRDF effects on $M_{\rm cr}$ for a moderately polluted troposphere as a function of VZA along the principal plane. In the backward scattering direction, BRDF $M_{\rm cr}$ is higher by 5-20%. The higher surface BRDF reflectance and TOA reflectance makes the retrieval more sensitive to the NO_2 in the boundary layer. In the forward scattering direction, BRDF $M_{\rm cr}$ is lower by 5-15%.

Figure 9b shows surface BRDF effects on w and Fig. 9c shows the combined effect on total tropospheric M of changes in $M_{\rm cr}$ and in w in a partly cloudy scene with a $c_{\rm eff}$(Lamb.) = 0.1. In the backward scattering direction, tropospheric M is 9-30% higher when accounting for surface BRDF effects. The decrease in $c_{\rm eff}$ (and hence w) makes the retrieval more sensitive to the NO_2 below the cloud. In the forward scattering direction, tropospheric M is 14-22% lower when accounting for surface BRDF effects because of the stronger screening effect by the higher BRDF $c_{\rm eff}$. The surface BRDF effect on w enhances the effect on the clear-sky AMF by up to 10% in both the forward and backward scattering direction.

Figure 10 shows surface BRDF effects on total tropospheric M in partly cloudy scenes with increasing cloudiness for the specific combination of $(\theta, \theta_0) = (45^\circ, 30^\circ)$ in the principal plane, representative of typical GOME-2 or OMI measurements. For

Table 2. Settings for the Lambertian and BRDF tropospheric NO_2 AMF calculations shown in Fig. 9.

	Lambertian AMF	**BRDF AMF**
Surface parameters	$A_{\mathrm{ws}} = 0.036$	$(f_{\mathrm{iso}}, f_{\mathrm{vol}}, f_{\mathrm{geo}}) = (0.04, 0.03, 0.008)$
Cloud fraction	$c_{\mathrm{eff}}(\mathrm{Lamb.}) = 0.1$	Backward scat.: $c_{\mathrm{eff}}(\mathrm{BRDF}) = 0.1 - 0.05$ Forward scat.: $c_{\mathrm{eff}}(\mathrm{BRDF}) = 0.1 + 0.05$
Cloud radiance fraction	R'_{cr} , R'_{cd}, $c_{\mathrm{eff}}(\mathrm{Lamb.})$	R_{cr} , R_{cd}, $c_{\mathrm{eff}}(\mathrm{BRDF})$
	Common settings	
Atmospheric profile	Mid latitude standard atmosphere Surface pressure: P_s= 1013 hPa	
NO_2 tropospheric column	Moderately polluted: $N_{\mathrm{v,trop}} = 4 \cdot 10^{15}$ molec·cm^{-2} Unpolluted: $N_{\mathrm{v,trop}} = 0.2 \cdot 10^{15}$ molec·cm^{-2}	
Lambertian cloud (IPA)	Cloud albedo: A_{cd} = 0.8 Cloud pressure: P_{cd} = 850 hPa	

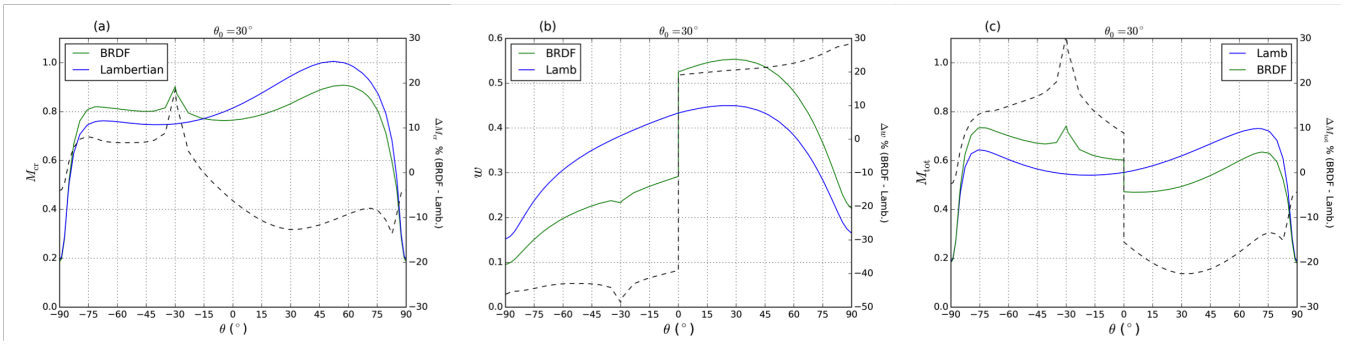

Figure 9. (a) Clear-sky tropospheric NO_2 AMF, (b) cloud radiance fraction and (c) total tropospheric NO_2 AMF computed with surface BRDF (green) and with a Lambertian surface (blue) and their relative difference (right axis) as a function of viewing zenith angle in the principal plane ($\varphi - \varphi_0$ = 180° for negative θ and $\varphi - \varphi_0$ = 0° for positive θ), for $\theta_0 = 30°$. P_{cd} = 850 hPa, Lambertian c_{eff} = 0.1 and BRDF c_{eff} = 0.10 ± 0.05. Surface BRDF parameters are (f_{iso}, f_{vol}, f_{geo}) = (0.04, 0.03, 0.008) and A_{ws} = 0.036 for the Lambertian surface. Troposphere is moderately polluted ($N_{v,trop}$= $4 \cdot 10^{15}$ molec·cm^{-2}).

a polluted troposphere (represented by stars), the total effect of accounting for surface BRDF is to increase M in the backward scattering direction (Fig. 10a) and to reduce M in the forward scattering direction (Fig. 10b). Average relative differences of about 15% for M_{cr} increase up to 25-40% for low cloud fractions (below 0.1) (see Fig. S5 in the supplementary material). The effect decreases for higher cloud fractions, with relative differences below 10% for cloud fractions higher than 0.5. For a lower bias in c_{eff} (e.g. 0.02), the effect on M reduces to about 15-20%, which is still a considerable effect.

For an unpolluted troposphere, surface BRDF effects on M_{cr} are in the same direction as in the polluted case but smaller (-7 to +11%). In a partly cloudy scene, Lambertian and BRDF tropospheric M are similar within -3 to 7%. Because there is

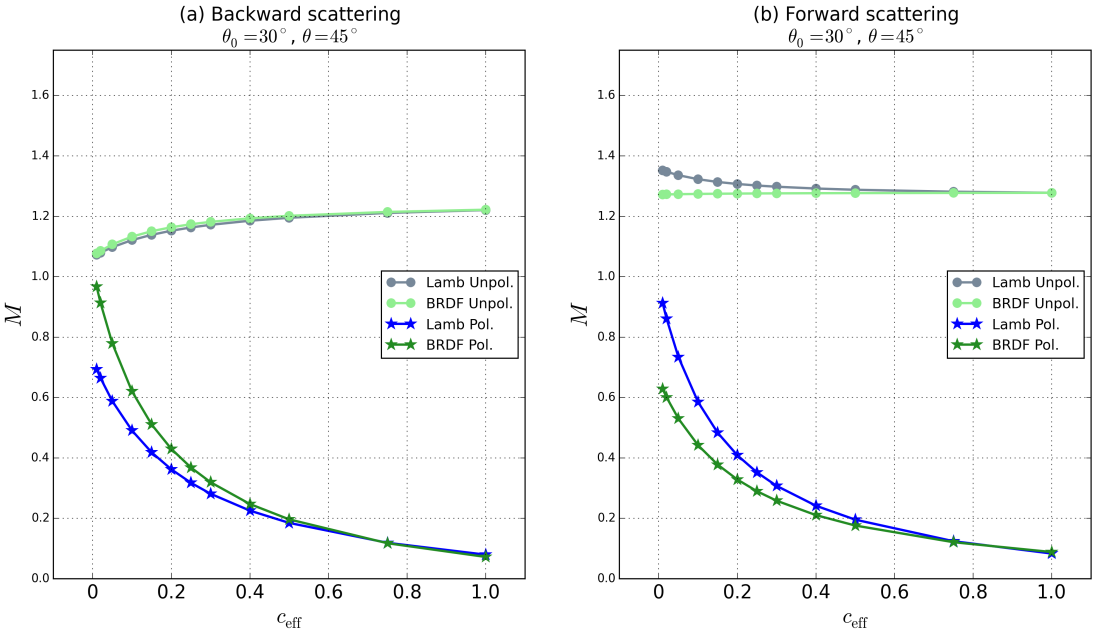

Figure 10. Total tropospheric NO_2 AMF as a function of cloud fraction in the (a) backward scattering direction and (b) forward scattering direction computed with surface BRDF (green) and a Lambertian surface (blue), for P_{cd} = 850 hPa, (θ, θ_0) = (45°, 30°), for a moderately polluted (stars) and unpolluted (circles) troposphere. BRDF parameters are (f_{iso}, f_{vol}, f_{geo}) = (0.04, 0.03, 0.008) and A_{ws} = 0.036 for the Lambertian surface.

very little NO_2 below the cloud, the effect of change in w counteracts (and largely cancels) the effect on the clear-sky AMF (circles in Fig. 10). The differences between BRDF and Lambertian AMF for different cloud pressures are shown in Fig. S6 in the supplementary material. A preliminary analysis done with a directional surface LER derived from GOME-2 shows that accounting for surface reflectance anisotropy effects reduces the cloud pressure by 40 hPa on average (with differences up to 120 hPa). This means that high cloud fractions will occur less often and therefore the results shown for 850 hPa are representative of the surface BRDF effects on AMFs.

5.2 GOME-2A tropospheric NO_2 air mass factors

We calculate Lambertian and BRDF NO_2 tropospheric AMFs for the exact illumination and viewing geometries of GOME-2A measurements over Amazonia and over France for March 2008. This results in approximately 1300 clear-sky pixels analyzed over Amazonia and 700 over France. We assume a moderately polluted atmosphere in every scene and colocate MODIS pixels with the GOME-2A pixel centre to obtain the surface BRDF parameters. For the Lambertian simulations, we use the surface LER value of each pixel from the GOME-2 climatology. We apply Lambertian and BRDF c_{eff} distributions from Sect. 4.2 (as

in Fig. 8). This way we account for the calculated surface BRDF effects in cloud fraction instead of the average change of 0.05 assumed in the sensitivity analysis in Sect. 5.1.

Figure 11a shows that for East measurements (i.e., forward scattering), $M_{\rm cr}$ decreases on average by 18% over Amazonia. Over France the decrease is on average 8% (not shown). Figure 11b shows that for West measurements (i.e., backward scattering), $M_{\rm cr}$ increases on average 5% over Amazonia and 7% over France, consistent with our findings in Fig. 9a. The differences of 15%-23% found in this analysis agree with the reported differences of 10%-20% in Noguchi et al. (2014) and Zhou et al. (2010) for clear-sky AMFs. The higher BRDF AMFs in the upper right corner of our study area correspond to a savanna ecosystem that is brighter than the dense rainforest. Because of the higher resolution of the MODIS BRDF dataset, this feature is well captured and leads to higher AMFs both in the East and West measurements (see Fig. S2 in the supplementary material). MODIS albedo is able to capture spatial variability at scales that satellites with coarser pixels cannot (Russell et al., 2011).

Figure 11c shows that for East measurements (i.e., forward scattering), total tropospheric AMFs including surface BRDF effects on cloud fractions are on average 10% lower over Amazonia. The decrease is on average 7% over France (not shown). For West measurements, (i.e., backward scattering), total AMFs are on average 16% higher over both Amazonia (Fig. 11d) and France, illustrating that the $M_{\rm cr}$ effect is enhanced by the effect on the cloud fraction by 10%-15% on average. Vasilkov et al. (2017) also found increased differences in the tropospheric AMFs due to surface BRDF effects on cloud parametes, but as reported by Lin et al. (2014), there can also be compensating effects.

These results show that surface BRDF affects both clear-sky AMF and cloud radiance fractions, which in combination significantly affect total NO_2 AMFs. As shown in Fig. 11, the sign and magnitude of the surface BRDF effects show strong spatial variations. Over ~~rough~~ forested terrain, current tropospheric AMF are likely underestimated in the backscatter regime and overestimated in the forward scattering regime by up to 25-35%, explained by systematic errors in $M_{\rm cr}$ and w. These results show that surface BRDF effects have to be included consistently in both cloud and trace gas retrievals.

6 Discussion and conclusions

We analyzed the effects of surface reflectance anisotropy on the OMI and GOME-2 satellite retrievals of cloud parameters and tropospheric NO_2 columns that currently use Lambertian-equivalent reflectivity (LER) climatologies. These climatologies, and consequently retrieved cloud fractions, show substantial across-track biases over terrain with a strong BRDF directionality. Here we interpret these with the DAK radiative transfer model. A clear understanding of the reasons for the biases and how they propagate in the tropospheric NO_2 column retrieval is critical to improve cloud and trace gas retrieval algorithms for satellite sensors.

An important finding is that the LER climatologies slightly overestimate surface albedo for forward scattering satellite viewing geometries (eastern part of GOME-2 orbit), and highly underestimate the surface albedo for backscatter viewing geometries (western part). The underestimation is as large as a factor of 2 over ~~vegetated~~ forested scenes in the near-infrared (772 nm). They are weaker but still relevant in the visible (494 nm), where surfaces are darker and Rayleigh scattering effects

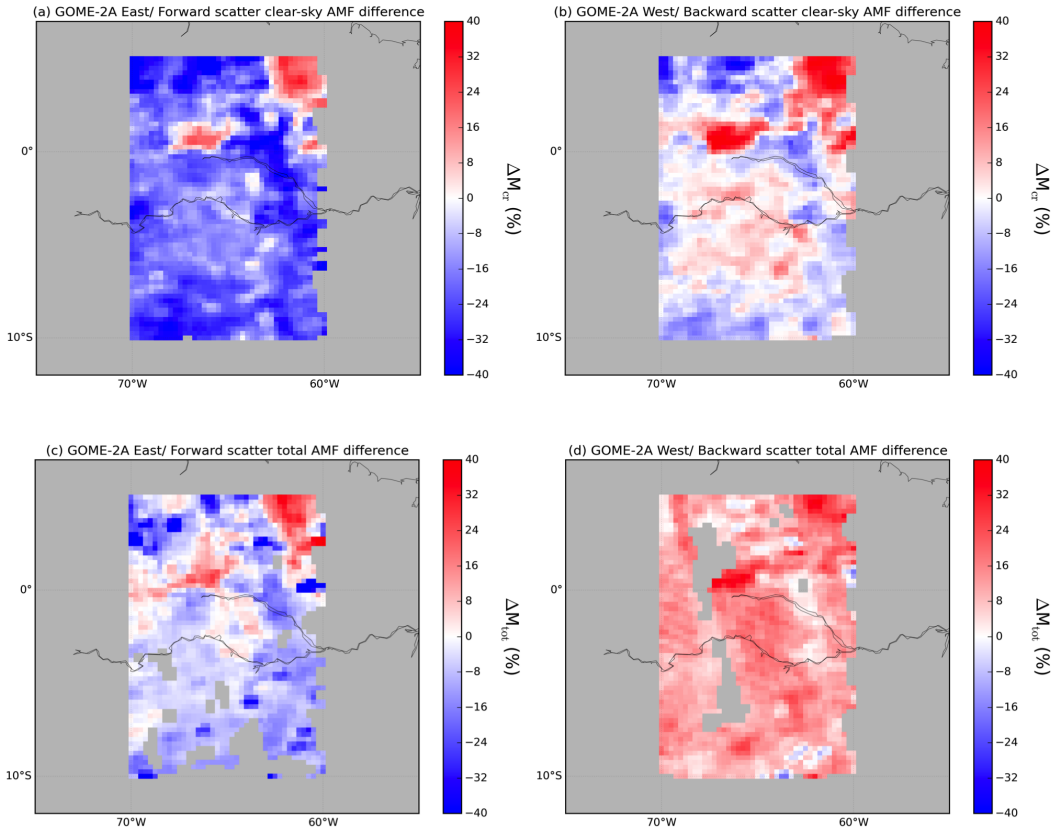

Figure 11. Relative differences between BRDF and Lambertian AMFs over Amazonia for March 2008: (a) clear-sky tropospheric NO_2 AMFs for East GOME-2A measurements (forward scatter) (b) clear-sky tropospheric NO_2 AMFs for West GOME-2A measurements (backward scatter) (c) total tropospheric NO_2 AMF for East GOME-2A measurements (forward scatter) and (d) total tropospheric NO_2 AMF for West GOME-2A measurements (backward scatter). Total AMFs are only shown for $c_{\mathrm{eff}} < 0.5$.

are stronger. Such across-track bias in surface LER propagates into the cloud fraction retrievals: we find biases in cloud fractions of up to 50% between backscatter and forward scattering geometries in the GOME-2 FRESCO and 26% in the OMI OMCLDO2 cloud algorithms. Time-of-day does not drive importance of surface BRDF effects, but specific viewing geometry and spectral range do.

To interpret the above biases, we extended the description of surface reflectance in DAK to include the geometrical surface reflecting properties via the Bidirectional Reflectance Distribution Function (BRDF) from the Ross-Li semi-empirical model. This allows DAK to simulate not only isotropic reflection at the surface, but also the anisotropic contributions from volumetric (e.g. leaf scattering) and from geometric (e.g. shadow-casting) effects. We evaluated DAK top-of-atmosphere (TOA) reflectance

simulations against other radiative transfer models, and find agreement within 1% between DAK and SCIATRAN, even within the so-called "hot-spot" backscatter reflectance peak. We then simulated TOA reflectances over vegetated scenes using BRDF parameters from a daily, high-resolution database derived from 16-years of MODIS measurements recently developed within the QA4ECV-project (QA4ECV-WP4, 2016). Our updated DAK simulations show considerably higher TOA reflectance levels for backscatter viewing geometries than those with isotropic surface reflection (LER) only. This strongly hints that across-track biases in cloud fractions can be explained by the lack of a description of surface reflectance anisotropy in the FRESCO and OMCLDO2 algorithms.

Subsequent sensitivity tests indicated that accounting for surface reflectance anisotropy in the FRESCO and OMCLDO2 retrieval framework removes the bias in cloud fractions. A correct physical description of surface anisotropy is essential for FRESCO, because cloud properties are retrieved in the NIR spectral range (760-790 nm) where surface BRDF effects are stronger and the atmosphere is virtually transparent. It is also of high relevance for scenes with low cloud fractions, where trace gas retrievals are still sensitive to pollution close to the ground. A discussion on the validity of the Lambertian cloud model is beyond the scope of this study. Nevertheless, the cloud fraction dependency with VZA for cloudy scenes suggests that the use of a more realistic cloud model should be considered in future improvements of cloud retrievals.

The implications for NO_2 air mass factor (AMF) calculations are substantial. Total tropospheric NO_2 AMFs are calculated as the radiative cloud fraction-weighted sum of cloudy and clear-sky AMFs. For moderately polluted NO_2 and backscatter geometries, we find that clear-sky AMFs are up to 20% higher and cloud radiance fractions up to 40% lower if surface reflectance anisotropic effects are accounted for. The combined effect of these changes is that NO_2 AMFs in polluted situations increase by 25-30% for backscatter geometries (and decrease by 25-35% for forward scattering geometries), stronger than the effect of either contribution alone.

An issue that was not addressed in this study is the role of aerosols. Noguchi et al. (2014) showed that scattering by aerosols generally dampens surface BRDF effects for clear-sky scenes. However, more research is needed to assess how specific aerosol characteristics (i.e. aerosol amount and type, vertical distribution relative to cloud) will affect cloud parameter retrievals and air mass factor calculations both in clear-sky and cloudy conditions.

We conclude that it is necessary to coherently account for surface reflectance anisotropy effects in retrievals of cloud properties and trace gases from UV/vis satellite sensors. A number of recent studies have attempted to account for the effects of anisotropic reflectance on both cloud and NO_2 retrievals (Lin et al. (2014); Vasilkov et al. (2017)), but a global assessment including the full range of possible retrieval conditions is still missing. An additional incentive to account for surface reflectance anisotropy is that the currently available LER climatologies (Kleipool et al. (2008); Tilstra et al. (2017)) describe the spatial variation in albedo at a scale (0.5°×0.5° - 1°×1°) coarser than the OMI or GOME-2 pixel itself (13 × 24 km^2 / 80 × 40 km^2). Using these coarse LER climatologies in AMF calculations degrades the intrinsic spatial resolution of the satellite retrievals, an issue that will be exacerbated for the recently launched TROPOMI instrument, with pixels as small as 3.5×7 km^2. A viable alternative to the current LER climatologies is provided by the MODIS-derived BRDF-parameters at a spatial resolution better than the GOME-2, OMI, and TROPOMI pixel sizes. MODIS Terra and Aqua are expected to last until 2025 and afterwards the Joint Polar Satellite System (JPSS) satellite constellation assures continuity of land observations needed to produce surface

BRDF data. Sentinel-3 could be employed to generate a BRDF similar to the one from the ESA GlobAlbedo broadband and the QA4ECV spectral albedo after some years of measurements. Another alternative is to make a directionally dependent LER database from TROPOMI once there is enough surface reflectance data acquired by the satellite itself.

Appendix A: Kernels for the Ross-Li BRDF model

We summarize here the expressions of the kernels implemented in DAK to model the surface reflectance anisotropy. We refer the reader to the original literature where these kernels were derived for more detailed information.

A1 Ross-Thick kernel

The expression of the Ross-Thick volumetric scattering kernel is (Roujean et al., 1992):

$$K_{\mathrm{vol}} = [\frac{(\pi/2-\xi)\cos\xi+\sin\xi}{\cos\theta'+\cos\theta}]\cdot[1+(1+\xi/\xi_0)^{-1}]-\frac{\pi}{4}. \tag{A1}$$

Here θ and θ' are the incident and reflected zenith angles, respectively. ξ is the scattering angle defined as:

$$cos\xi = \cos\theta\cos\theta'+\sin\theta\sin\theta'\cos(\varphi-\varphi') \tag{A2}$$

where $\varphi-\varphi'$ is the relative azimuth angle (viewing and solar azimuth difference).

The term in the second squared bracket in Eq. A1 is the modified part for the hot-spot modelling, where ξ_0 is the hot spot characteristic angle (typically 1.5°). This characteristic angle can be related to the ratio of the size of scattering element and the canopy vertical density (Maignan et al., 2004).

A2 Li-Sparse kernel

The expression of the Li-Sparse geometric scattering kernel is (Li and Strahler (1986), Wanner et al. (1995)):

$$K_{\mathrm{geo}} = O(\theta,\theta',\varphi-\varphi')-\sec\theta^*-\sec\theta'^*+\frac{1}{2}(1+\cos\xi^*)\sec\theta^*\sec\theta'^*. \tag{A3}$$

The different terms in the equations are:

$$O = \frac{1}{\pi}(t-\sin t\cos t)(\sec\theta^*+\sec\theta'^*), \tag{A4}$$

$$\cos t = \frac{h}{b}\frac{\sqrt{D^2+(\tan\theta'^*\tan\theta^*\sin(\varphi-\varphi'))^2}}{\sec\theta^*\sec\theta'^*}, \qquad D=\sqrt{\tan^2\theta^*+\tan^2\theta'^*+2\tan\theta^*\tan\theta'^*\cos(\varphi-\varphi')}. \tag{A5}$$

The angles with a star are equivalent angles to convert spheroids-like object to spheres:

$$\theta^* = \tan^{-1}(\frac{b}{r}\tan\theta), \quad \theta'^* = \tan^{-1}(\frac{b}{r}\tan\theta'). \tag{A6}$$

O (Eq. A4) is the overlap area between the shadow of illumination and the shadow of viewing projections on the ground. D is the distance between the centers of the scattering objects. The parameter t is used to parametrize the scattering objects spherically. This kernel it is not linear as it has two parameters $\frac{b}{r}$ and $\frac{h}{b}$ describing the shape and the relative height of the scattering objects.

Competing interests. The authors declare that they have no conflict of interest.

Acknowledgements. This research has been supported by the EU FP7 Project Quality Assurance for Essential Climate Variables (QA4ECV), grant no. 607405. We acknowledge the free use of the GOME-2 data provided by EUMETSAT.

References

Air quality in Europe - 2016 Report, Tech. Rep. 28/2016, TH-AL-16-127-EN-N, European Environmental Agency, EEA, https://doi.org/10.2800/80982, 2016.

Acarreta, J. R., De Haan, J. F., and Stammes, P.: Cloud pressure retrieval using the O2-O2 absorption band at 477 nm, J. Geophys. Res.: Atmospheres, 109, n/a–n/a, https://doi.org/10.1029/2003JD003915, d05204, 2004.

Boersma, K. F., Eskes, H. J., and Brinksma, E. J.: Error analysis for tropospheric NO_2 retrieval from space, J. Geophys. Res., 109, D04 311, https://doi.org/10.1029/2003JD003962, 2004.

Boersma, K. F., Eskes, H. J., Dirksen, R. J., van der A, R. J., Veefkind, J. P., Stammes, P., Huijnen, V., Kleipool, Q. L., Sneep, M., Claas, J., Leitao, J., Richter, A., Zhou, Y., and Brunner, D.: An improved tropospheric NO_2 column retrieval algorithm for the Ozone Monitoring Instrument, Atmos. Meas. Tech., 4, 1905–1928, https://doi.org/10.5194/amt-4-1905-2011, 2011.

Bucsela, E. J., Krotkov, N. A., Celarier, E. A., Lamsal, L. N., Swartz, W. H., Bhartia, P. K., Boersma, K. F., Veefkind, J. P., Gleason, J. F., and Pickering, K. E.: A new stratospheric and tropospheric NO_2 retrieval algorithm for nadir-viewing satellite instruments: applications to OMI, Atmos. Meas. Tech., 6, 2607–2626, https://doi.org/10.5194/amt-6-2607-2013, 2013.

Camacho-de Coca, F., Bréon, F. M., Leroy, M., and Garcia-Haro, F. J.: Airborne measurement of hot spot reflectance signatures, Remote Sensing of Environment, 90, 63 – 75, https://doi.org/https://doi.org/10.1016/j.rse.2003.11.019, 2004.

de Haan, J. F., Bosma, P. B., and Hovenier, J. W.: The adding method for multiple scattering calculations of polarized light, Astron. Astrophys, 183, 371–391, 1987.

De Smedt, I., Theys, N., Yu, H., Danckaert, T., Lerot, C., Compernolle, S., Van Roozendael, M., Richter, A., Hilboll, A., Peters, E., Pedergnana, M., Loyola, D., Beirle, S., Wagner, T., Eskes, H., van Geffen, J., Boersma, K. F., and Veefkind, P.: Algorithm Theoretical Baseline for formaldehyde retrievals from S5P TROPOMI and from the QA4ECV project, Atmos. Meas. Tech. Discuss., 2017, 1–53, https://doi.org/10.5194/amt-2017-393, 2017.

Kleipool, Q. L., Dobber, M. R., de Haan, J. F., and Levelt, P. F.: Earth surface reflectance climatology from 3 years of OMI data, J. Geophys. Res.: Atmospheres, 113, https://doi.org/10.1029/2008JD010290, d18308, 2008.

Koelemeijer, R. B. A., Stammes, P., Hovenier, J. W., and de Haan, J. F.: Global distributions of effective cloud fraction and cloud top pressure derived from oxygen A band spectra measured by the Global Ozone Monitoring Experiment: Comparison to ISCCP data, J. Geophys. Res.: Atmospheres, 107, AAC 5–1–AAC 5–9, https://doi.org/10.1029/2001JD000840, 2002.

Koelemeijer, R. B. A., de Haan, J. F., and Stammes, P.: A database of spectral surface reflectivity in the range 335–772 nm derived from 5.5 years of GOME observations, J. Geophys. Res.: Atmospheres, 108, n/a–n/a, https://doi.org/10.1029/2002JD002429, 4070, 2003.

Lamsal, L. N., Martin, R. V., van Donkelaar, A., Steinbacher, M., Celarier, E. A., Bucsela, E., Dunlea, E. J., and Pinto, J. P.: Ground-level nitrogen dioxide concentrations inferred from the satellite-borne Ozone Monitoring Instrument, J. Geophys. Res.: Atmospheres, 113, https://doi.org/10.1029/2007JD009235, d16308, 2008.

Li, X. and Strahler, A. H.: Geometric-Optical Bidirectional Reflectance Modeling of a Conifer Forest Canopy, IEEE Trans. Geo. Rem. Sens., GE-24, 906–919, https://doi.org/10.1109/TGRS.1986.289706, 1986.

Lin, J.-T., Martin, R. V., Boersma, K. F., Sneep, M., Stammes, P., Spurr, R., Wang, P., Van Roozendael, M., Clémer, K., and Irie, H.: Retrieving tropospheric nitrogen dioxide from the Ozone Monitoring Instrument: effects of aerosols, surface reflectance anisotropy, and vertical profile of nitrogen dioxide, Atmos. Chem. Phys., 14, 1441–1461, https://doi.org/10.5194/acp-14-1441-2014, 2014.

Litvinov, P., Hasekamp, O., Cairns, B., and Mishchenko, M. I.: Semi-empirical BRDF and BPDF models applied to the problem of aerosol retrievals over land: testing on airborne data and implications for modeling of top-of-atmosphere measurements, pp. 313–340, Springer Netherlands, https://doi.org/10.1007/978-94-007-1636-0_13, 2011.

Lorente, A., Boersma, K. F., Yu, H., Dörner, S., Hilboll, A., Richter, A., Liu, M., Lamsal, L. N., Barkley, M., De Smedt, I., Van Roozendael, M., Wang, Y., Wagner, T., Beirle, S., Lin, J.-T., Krotkov, N., Stammes, P., Wang, P., Eskes, H. J., and Krol, M.: Structural uncertainty in air mass factor calculation for NO_2 and HCHO satellite retrievals, Atmos. Meas. Tech., 10, 759–782, https://doi.org/10.5194/amt-10-759-2017, 2017.

Maignan, F., Bréon, F.-M., and Lacaze, R.: Bidirectional reflectance of Earth targets: evaluation of analytical models using a large set of spaceborne measurements with emphasis on the Hot Spot, Remote Sensing of Environment, 90, 210 – 220, https://doi.org/http://doi.org/10.1016/j.rse.2003.12.006, 2004.

Martin, R. V., Jacob, D. J., Chance, K., Kurosu, T. P., Palmer, P. I., and Evans, M. J.: An improved retrieval of tropospheric nitrogen dioxide from GOME, J. Geophys. Res., 107, 4437, https://doi.org/10.1029/2001JD001027, 2002.

Martin, R. V., Jacob, D. J., Chance, K.and Kurosu, T. P., Palmer, P. I., and Evans, M. J.: Global inventory of nitrogen oxide emissions constrained by space-based observations of NO2 columns, J. Geophys. Res.: Atmospheres, 108, https://doi.org/10.1029/2003JD003453, http://dx.doi.org/10.1029/2003JD003453, 4537, 2003.

MCD43A1: MODIS/Terra and Aqua BRDF/Albedo Model Parameters Daily L3 Global 500 m SIN Grid V006, https://doi.org/DOI: 10.5067/MODIS/MCD43A1.006, https://ladsweb.nascom.nasa.gov/api/v1/productPage/product=MCD43A1.

Myhre, G., Kvalevåg, M. M., and Schaaf, C. B.: Radiative forcing due to anthropogenic vegetation change based on MODIS surface albedo data, Geophysical Research Letters, 32, n/a–n/a, https://doi.org/10.1029/2005GL024004, l21410, 2005.

Nicodemus, F. E., Richmond, J. C., Hsia, J. J., Ginsberg, I. W., and Limperis, T.: in: Radiometry, edited by Wolff, L. B., Shafer, S. A., and Healey, G., chap. Geometrical Considerations and Nomenclature for Reflectance, pp. 94–145, Jones and Bartlett Publishers, Inc., USA, 1992.

Noguchi, K., Richter, A., Rozanov, V., Rozanov, A., Burrows, J. P., Irie, H., and Kita, K.: Effect of surface BRDF of various land cover types on geostationary observations of tropospheric NO_2, Atmos. Meas. Tech., 7, 3497–3508, https://doi.org/10.5194/amt-7-3497-2014, 2014.

Oleson, K. W., Bonan, G. B., Schaaf, C., Gao, F., Jin, Y., and Strahler, A.: Assessment of global climate model land surface albedo using MODIS data, Geophysical Research Letters, 30, n/a–n/a, https://doi.org/10.1029/2002GL016749, 1443, 2003.

QA4ECV-WP4: Product User Guide for Land ECVs and Product Specification Document for Atmosphere ECV precursors. Part 1: Product User Guide for QA4ECV-albedo, Deliverable 4.6, 2016.

Richter, A., Burrows, J. P., Nusz, H., Granier, C., and Niemeier, U.: Increase in tropospheric nitrogen dioxide over China observed from space, Nature, 437, 129–132, https://doi.org/10.1038/nature04092, 2005.

Roujean, J.-L., Leroy, M., and Deschamps, P.-Y.: A bidirectional reflectance model of the Earth's surface for the correction of remote sensing data, J. Geophys. Res., 97, 20 455–20 468, https://doi.org/10.1029/92JD01411, 1992.

Rozanov, V. V., Rozanov, A. V., Kokhanovsky, A. A., and Burrows, J. P.: Radiative tranfer through terrestrial atmosphere and ocean: Software package SCIATRAN, J. Quant. Spectrosc. Radiat. Transfer, 133, 13–71, https://doi.org/10.1016/j.jqsrt.2013.07.004, 2014.

Russell, A. R., Perring, A. E., Valin, L. C., Bucsela, E. J., Browne, E. C., Wooldridge, P. J., and Cohen, R. C.: A high spatial resolution retrieval of NO_2 column densities from OMI: method and evaluation, Atmos. Chem. Phys., 11, 8543–8554, https://doi.org/10.5194/acp-11-8543-2011, 2011.

Schaepman-Strub, G., Schaepman, M., Painter, T., Dangel, S., and Martonchik, J.: Reflectance quantities in optical remote sensing—definitions and case studies, Remote Sensing of Environment, 103, 27 – 42, https://doi.org/https://doi.org/10.1016/j.rse.2006.03.002, 2006.

Spurr, R. J. D.: A new approach to the retrieval of surface properties from earthshine measurements, J. Quant. Spectrosc. Radiat. Transfer, 83, 15 – 46, https://doi.org/http://doi.org/10.1016/S0022-4073(02)00283-2, 2004.

Stammes, P., de Haan, J. F., and Hovenier, J. W.: The polarized internal radiation field of a planetary atmosphere, Astron. Astrophys., 225, 239–259, 1989.

Stammes, P., Sneep, M., de Haan, J. F., Veefkind, J. P., Wang, P., and Levelt, P. F.: Effective cloud fractions from the Ozone Monitoring Instrument: Theoretical framework and validation, J. Geophys. Res.: Atmospheres, 113, n/a–n/a, https://doi.org/10.1029/2007JD008820, d16S38, 2008.

Strahler, A. H., Lucht, W., Schaaf, C. B., Tsang, T., Gao, F., Li X.and Muller, J. P., Lewis, P., and Barnsley, M. J.: MODIS BRDF/Albedo Product: Algorithm Theoretical Basis Document Version 5.0. MODIS Product ID: MOD43, 1999.

Tilstra, L. G., Tuinder, O. N. E., Wang, P., and Stammes, P.: Surface reflectivity climatologies from UV to NIR determined from Earth observations by GOME-2 and SCIAMACHY, J. Geophys. Res.: Atmospheres, 122, 4084–4111, https://doi.org/10.1002/2016JD025940, 2016JD025940, 2017.

Torres, O., Tanskanen, A., Veihelmann, B., Ahn, C., Braak, R., Bhartia, P. K., Veefkind, P., and Levelt, P.: Aerosols and surface UV products from Ozone Monitoring Instrument observations: An overview, J. Geophys. Res.: Atmospheres, 112, https://doi.org/10.1029/2007JD008809, d24S47, 2007.

Vasilkov, A., Qin, W., Krotkov, N., Lamsal, L., Spurr, R., Haffner, D., Joiner, J., Yang, E.-S., and Marchenko, S.: Accounting for the effects of surface BRDF on satellite cloud and trace-gas retrievals: a new approach based on geometry-dependent Lambertian equivalent reflectivity applied to OMI algorithms, Atmos. Meas. Tech., 10, 333–349, https://doi.org/10.5194/amt-10-333-2017, 2017.

Veefkind, J. P., de Haan, J. F., Sneep, M., and Levelt, P. F.: Improvements to the OMI O_2–O_2 operational cloud algorithm and comparisons with ground-based radar–lidar observations, Atmos. Meas. Tech., 9, 6035–6049, https://doi.org/10.5194/amt-9-6035-2016, 2016.

Vermote, E. F. and Kotchenova, S.: Atmospheric correction for the monitoring of land surfaces, J. Geophys. Res.: Atmospheres, 113, n/a–n/a, https://doi.org/10.1029/2007JD009662, d23S90, 2008.

Vermote, E. F., El Saleous, N., Justice, C. O., Kaufman, Y. J., Privette, J. L., Remer, L., Roger, J. C., and Tanré, D.: Atmospheric correction of visible to middle-infrared EOS-MODIS data over land surfaces: Background, operational algorithm and validation, J. Geophys. Res.: Atmospheres, 102, 17 131–17 141, https://doi.org/10.1029/97JD00201, http://dx.doi.org/10.1029/97JD00201, 1997.

Wang, P., Stammes, P., van der A, R., Pinardi, G., and van Roozendael, M.: FRESCO+: an improved O_2 A-band cloud retrieval algorithm for tropospheric trace gas retrievals, Atmos. Chem. Phys., 8, 6565–6576, https://doi.org/10.5194/acp-8-6565-2008, 2008.

Wanner, W., Li, X., and Strahler, A. H.: On the derivation of kernels for kernel-driven models of bidirectional reflectance, J. Geophys. Res., 100, 21 077–21 089, https://doi.org/10.1029/95JD02371, 1995.

Zhou, Y., Brunner, D., Spurr, R. J. D., Boersma, K. F., Sneep, M., Popp, C., and Buchmann, B.: Accounting for surface reflectance anisotropy in satellite retrievals of tropospheric NO_2, Atmos. Meas. Tech., 3, 1185–1203, https://doi.org/10.5194/amt-3-1185-2010, 2010.